Ore Geology Reviews 141 (2022) 104682

Contents lists available at ScienceDirect

Ore Geology Reviews

journal homepage: www.elsevier.com/locate/oregeorev

Genetic model for early Cambrian reef limestone-hosted Pb-Zn deposits in the world-class Huayuan orefield, South China: New insights from mineralogy, fluorite geochemistry and sulfides in situ S-Pb isotopes

Yusi Hu [a], Lin Ye [a,*], Zhilong Huang [a,*], Chen Wei [a,b], Tao Wu [a,b], Zhenzhong Xiang [a,b], Shiyu Liu [a,c], Zhenli Li [a,b]

[a] State Key Laboratory of Ore Deposit Geochemistry, Institute of Geochemistry, Chinese Academy of Sciences, Guiyang 550081, China
[b] University of Chinese Academy of Sciences, Beijing 100049, China
[c] College of Resources and Environmental Engineering, Guizhou University, Guiyang 550081, China

ARTICLE INFO

Keywords:
LA-(MC)-ICPMS
Sources of sulfur and metals
Sulfide depositional mechanism
Ore genesis
Genetic model

ABSTRACT

The Xiangxi-Qiandong metallogenic belt (>300 Mt sulfide ores @~4.0 wt% Pb + Zn), located at the southeastern margin of the Yangtze Block, is one of the important Pb-Zn producers in China. Although carbonate-hosted Pb-Zn deposits in this district have attracted great attention during past decades, many issues, particularly the ore genesis and geodynamic setting, remain unclear. In this study, we take the Limei and Yutang deposits as typical case studies, using detailed geology, rare earth elements and yttrium (REY) geochemistry of fluorite and sulfides in situ S-Pb isotopes, to propose a new model for early Cambrian reef limestone-hosted Pb-Zn deposits in the district. REY contents (0.47 to 8.67 ppm; mean = 3.99 ppm) in fluorite from Limei and Yutang slightly deplete in LREE and HREE relative to MREE, indicating that the REEs and metals were transported predominantly as chloride complexes in a low-temperature (<200 °C) hydrothermal fluid with high saline. New $\delta^{34}S$ values of sulfides (+27.66 to + 35.46‰ in Limei and + 24.80 to + 36.07‰ in Yutang) imply that S^{2-} was originated from evaporite sulfate within ore-hosting strata via thermo-chemical reduction (TSR) as the presence of reducing agents (bioclastic limestone and organic matter). In situ $\delta^{34}S$ values show a slightly large range (variation up to 11.27‰) and vary significantly within single grain (up to 4.60‰), which may be inherited from the S composition of H_2S in the original fluid. In situ Pb isotopic ratios of sulfides from Limei ($^{206}Pb/^{204}Pb$ = 18.001–18.269, $^{207}Pb/^{204}Pb$ = 15.645–15.796 and $^{208}Pb/^{204}Pb$ = 38.243–38.597) and Yutang ($^{206}Pb/^{204}Pb$ = 18.135–18.384, $^{207}Pb/^{204}Pb$ = 15.714–15.924 and $^{208}Pb/^{204}Pb$ = 38.347–38.874) positively correlates in Pb-Pb diagrams, indicating the mineralizing metals are mainly derived from Proterozoic basement rocks with an amount of contribution from early Cambrian sedimentary rocks. Mineralogy, fluorite REY geochemistry and sulfides in situ S-Pb isotopes together with previously reported mineralization ages suggest that the mixing of metal-rich fluid from basement rocks and the H_2S-rich fluid originated from ore-hosting strata plays an important role in forming the Pb-Zn deposits of Limei and Yutang. This study provides a typical example for better understanding the genesis and geodynamic setting of MVT deposits in the foreland basin, South China.

1. Introduction

Mississippi valley-type (MVT) deposits are defined as epigenetic carbonate-hosted Pb-Zn deposits that have no genetic association with igneous activity. These deposits, one of the most important sediment-hosted Pb-Zn deposits, are globally distributed and are estimated to host 16 to 17% of the known global lead and zinc resources (Leach et al., 2005). The most famous ore district/deposits include the Upper Mississippi Valley, Central Tennessee and Old Lead Belt in USA (Leach and Rowan, 1986; Leach et al., 2005), Pine Point and Polaris in Canada (Powell and Macqueen, 1984; Randell and Anderson, 1996), Toussit-Bou Beker in Morocco (Bouabdellah et al., 1999), Upper Silesia in Poland (Heijlen et al. 2003) and the Pb-Zn metallogenic belts around the margins of Yangtze Block (e.g., Ye et al., 2011; Zhang et al., 2015; Zhou et al., 2018a,b; Leach and Song, 2019; Wei et al., 2021 and references therein). Extensive research has focused on the carbonate-hosted Pb-Zn

* Corresponding authors.
E-mail addresses: yelin@vip.gyig.ac.cn (L. Ye), huangzhilong@vip.gyig.ac.cn (Z. Huang).

https://doi.org/10.1016/j.oregeorev.2021.104682
Received 30 July 2021; Received in revised form 16 December 2021; Accepted 22 December 2021
Available online 27 December 2021

deposits around the margins of the Yangtze Block, particularly the Sichuan-Yunnan-Guizhou tringle and Sanjiang district, to document their geological characteristics, mineralization age, ore genesis and tectonic setting (e.g., Huang et al., 2004; Han et al., 2012; Hu et al., 2015; Zhou et al. 2018; Wei et al., 2021 and references therein). However, their counterparts in the Xiangxi-Qiandong metallogenic belt (XQMB) remain poorly investigated and understood (e.g., Duan, 2014)

The XQMB in South China hosts a number of carbonate-hosted Pb-Zn deposits with proven sulfide ores >300 Mt at an average grade of 4.0 wt % Pb + Zn (Wei, 2017), making it one of the most important lead and zinc production regions in China. Notably, the majority of the Pb-Zn deposits in the belt, including Limei, Yutang, Yangjiazhai, Shizishan, Danaopo, Xiunao, Bokouchang, Tanbianpo and Niujiaotang, are hosted by the early Cambrian Qingxudong Formation (Fm.). Among them, the two largest deposits are Limei (44.1 Mt sulfides @ 3.48% Zn and 0.22% Pb) and Yutang (131 Mt sulfides @ 3.18% Zn and 1.50% Pb) deposits show great economic importance. Many studies of the Pb-Zn metallogeny at Limei and Yutang, mostly published in Chinese or reported in student dissertations, have addressed the ore geology (e.g., Li, 1991; Duan, 2014), ore geochronology (Duan, 2014; Tan et al., 2018), fluid inclusions (Liu and Zheng, 2000; Zhou et al., 2018a,b) and bulk S-Pb isotope geochemistry (Zhou et al., 2016; Wei et al., 2017; Li, 2018). However, questions related to the sulfur and metal sources, the metal transport, and the genesis of the deposits remain debated. Several authors considered that these Pb-Zn deposits formed syngenetically with metals derived from ore-hosting strata (Luo et al., 2009; Chen et al., 2011) whereas Zhou et al. (2016) suggested an epigenetic origin controlled by structure. Other authors favored an initial syngenetic origin with subsequent modifications by later hydrothermal activity (Li, 1991; Mao, 2016).

Sulfur and lead isotopes are powerful indicators that can be used to constrain the sources of metals and fluid origin, as well as sulfide precipitation mechanism (Ohmoto and Rye, 1979; Schneider et al., 2002). Microanalytical techniques (e.g., LA-MC-ICPMS and SIMS) can provide high-precision elemental and/or isotope compositions at sub-micro scale that cannot be reflected by conventional bulk analytical methods (Peevler et al., 2003). Furthermore, the rare earth elements and yttrium (REY) geochemistry of fluorite can be an effective proxy for metal transport mechanisms because they are strongly affected by physical–chemical conditions (e.g., Bau et al., 2003)

In this contribution, we present the results of a comprehensive investigation of the Limei and Yutang deposits using detailed field investigation, ore mineralogy, trace elements in fluorite and in situ S and Pb isotopes. The goals are to (i) investigate the physical–chemical conditions and metal transport mechanisms, (ii) determine the chemistry of ore-forming fluids and sulfide precipitation mechanism, and (iii) evaluate the metal sources and the role of wall-rocks. This study, together with previous data, will contribute to a genetic model for the Limei and Yutang Pb-Zn deposits.

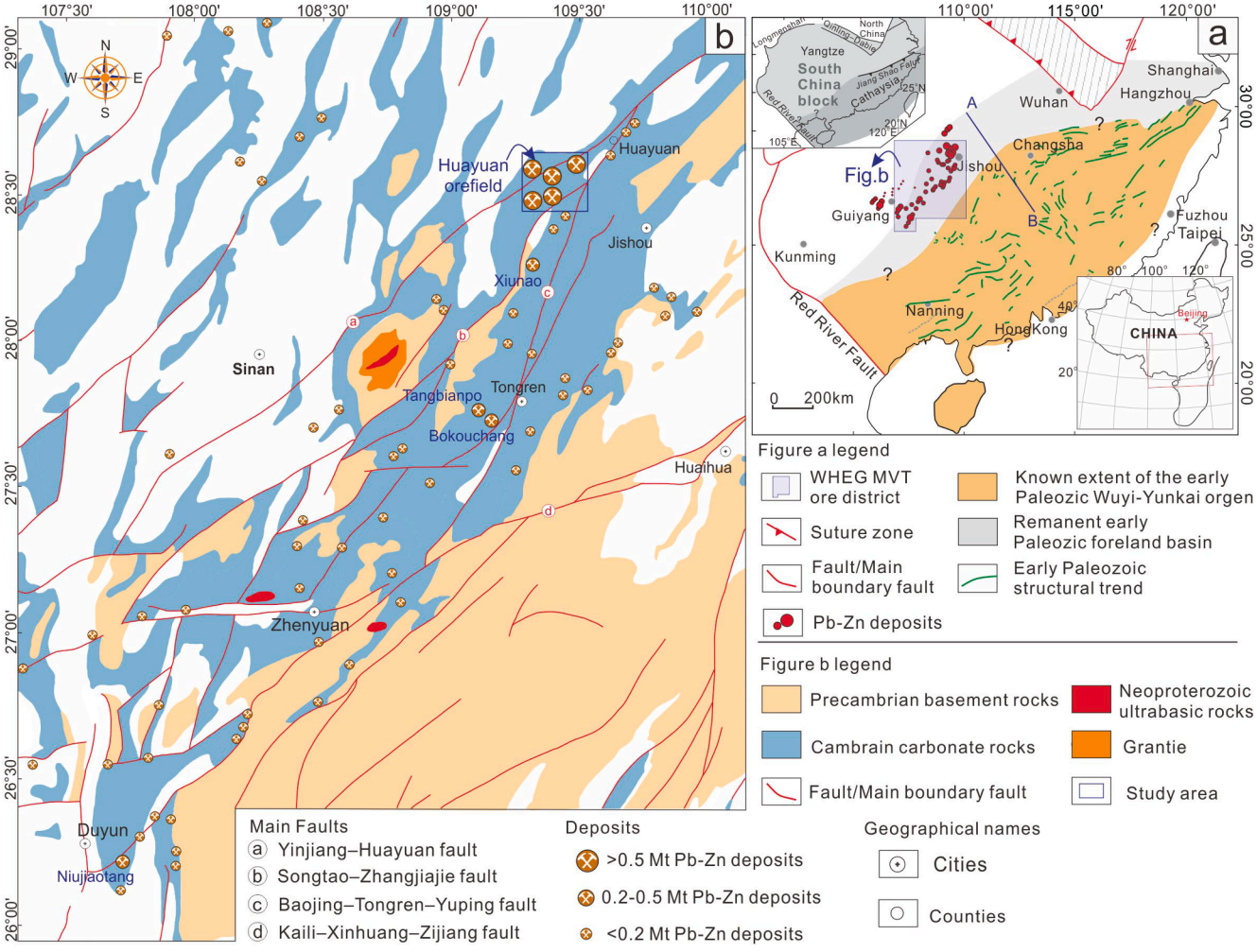

Fig. 1. (a) Simplified regional map of South China highlighting the regional extent of the early Paleozoic Wuyi–Yunkai orogeny and carbonate-hosted Pb-Zn deposits in the Xiangxi–Qiandong metallogenic belt (XQMB; modified from Li et al., 2010). Cross-section A-B is shown in Fig. 14a. (b) Geological map of the Xiangxi–Qiandong district showing the Pb-Zn deposit distribution, strata and regional faults (modified from Li, 2018).

2. Geological setting

2.1. Regional geology

The Yangtze Block, an important part of the South China Block, is bounded by the Qinling-Dabie, Sanjiang, Songpan–Ganzê and Cathaysia terranes to north, west, northwest and southwest, respectively (Fig. 1a). It comprises a late Paleoproterozoic to early Neoproterozoic crystalline basement made of metamorphosed sandstone–siltstone and silty slate, which is overlain by late Ediacaran to Quaternary sedimentary covers (Metcalfe, 2006).

Yangtze Block has experienced multiple tectonic events and has been described in detail by Metcalfe (2006) and Charvet (2013). From 850 to 820 Ma, the Yangtze Block and Cathaysia Block were amalgamated along the Jiangnan suture (e.g., Zhao et al., 2011). After ~ 820 Ma, a failed intracontinental rift system of Neoproterozoic age developed in the central (Nanhua rift) region of the South China Block and formed deep water sedimentary rocks of Neoproterozoic to Ordovician age (e.g., Wang and Li, 2003). During the Early Paleozoic (490–410 Ma) intracontinental Wuyi-Yunkai orogeny, the Nanhua rift evolved into a foreland basin (Yao and Li. 2016). In the early Triassic, the Cimmerian continental ribbons (i.e., Sibumasu) were accreted northward to the Indochina and South China blocks (e.g., Metcalfe, 2006). Concurrently, the South China Block collided with the North China Block along the Qingling-Dabie orogenic belt.

The XQMB is located at the southeastern margin of the Yangtze Block (Ye et al., 2011). Over 300 Pb-Zn known deposits of different sizes are hosted by the reef limestone of the Lower Cambrian Qingxudong Fm., although some are hosted in Late Ediacaran to Ordovician rocks. Four major NE- and NNE-trending regional fault belts, namely the Yinjiang–Huangyuan, the Songtao-Zhangjiajie, the Baojing–Tongren–Yuping and the Kaili–Xinhuang–Zijiang faults (Fig. 1b) controlled the distribution of the Pb-Zn deposits in the XQMB. These structures are well-developed and have been activated/re-activated by several orogenic events (Jiangnan, Wuyi–Yunkai, Indosinian and Yanshanian) occurring within the South China Block (e.g., Li et al., 2010; Wang et al., 2013). The XQMB is divided into two districts: the Xiangxi Pb-Zn district (>12.0 Mt Pb + Zn reserves) and the Qiandong Pb-Zn district (<1.0 Mt Pb + Zn reserves). The basic characteristic of the primary ore deposits in the two districts are summarized in Table 1.

2.2. The geology of the Huayuan orefield

The Huayuan orefield is located in the Xiangxi ore district, 45 km northwest of Jishou City (Fig. 2). More than 30 carbonate-hosted Pb-Zn deposits/prospects including Shizishan, Yutang, Limei, Danaopo and

Table 1
Basic geological characteristics of the primary Pb-Zn deposits in the Xiangxi-Qiandong metallogenic belt (XQMB).

Deposit	Metal assemblage	Geographical location	Hosting rocks	Metal resources (10^4 t)	Grade	Morphology of orebodies	Ore-controlling structure	Mineralization age (Ma)	Reference
The Xiangxi Pb-Zn district									
Danaopo	Pb-Zn(-Cd)	28° 32' N 109° 23' E	Lower Cambrian Qingxudong Fm. reef limestone	450.5,	Zn: 1.0–4.0%, Pb:0.1–0.8%,	Stratiform, stratoid and lense	Reef limestone	–	Mao, 2016; Wu et al., 2021
Limei	Pb-Zn(-Cd)	28° 31' N 109° 22' E	Lower Cambrian Qingxudong Fm. reef limestone	163.2	Zn: 3.48 %, Pb:0.22%	Stratiform, stratoid and veins	Reef limestone and NNE-trending faults	412 ± 6 (Sphalerite Rb-Sr)	Tan et al.,2018
Yutang	Pb-Zn(-Cd)	28° 26' N 109° 20' E	Lower Cambrian Qingxudong Fm. reef limestone	613	Zn: 3.18 %, Pb:1.50%	Stratiform, vein and breccia	Reef limestone	411 ± 10 (Sphalerite Rb-Sr)	Liu and Zheng 2000; Zhou et al., 2016;
Shizishan	Pb-Zn(-Cd)	28° 25' N 109° 18' E	Lower Cambrian Qingxudong Fm. reef limestone	94.0	Pb + Zn:~4.0%	Stratiform, vein and breccia	Reef limestone and NNE-trending fault	–	Duan, 2014
Yangjiazhai	Pb-Zn(-Cd)	28°29′ N, 109°21′ E	Lower Cambrian Qingxudong Fm. reef limestone	184.8	Pb + Zn: 2.79%,	Strataboundlenses	NE-trendingfaults	–	Wei, 2017; Hu et al., 2020
The Qiandong Pb-Zn district									
Xiunao	Pb-Zn	28° 13' N 109° 18' E	Lower Cambrian Qingxudong Fm. dolostone	<20	Zn:0.51–5.71%, Pb:0.58–1.95%,	Nest-like and lenses	NE-trending faults	–	Li, 2018
Tangbianpo	Pb-Zn	27° 42' N 109° 05' E	Lower Cambrian Qingxudong Fm. dolostone	>20	Zn: 2.31%, Pb:0.50%	Stratiform, stratoid and lense	Bioclastic limestone	477 ± 5 (Sphalerite Rb-Sr)	Yu et al., 2017
Bokouchang	Pb-Zn	27° 40' N 109° 07' E	Lower Cambrian Qingxudong Fm. dolostone	>20	Zn: 2.31%, Pb:0.5%	Stratiform and lentiform	Bioclastic limestone NE trending faults	422 ± 48 (Calcite Sm-Nd), 466 ± 13 (Sphalerite Rb-Sr)	Yang et al., 2015
Niujiaotang	Zn-Cd	26°07′ N, 107°65′ E	Lower Cambrian Qingxudong Fm. dolostone	~35	Zn: 3.75–6.62%, Cd: 0.01–0.20%	Stratoid and lenses	Wangsi anticline and NE-trending faults	–	Ye et al., 2012

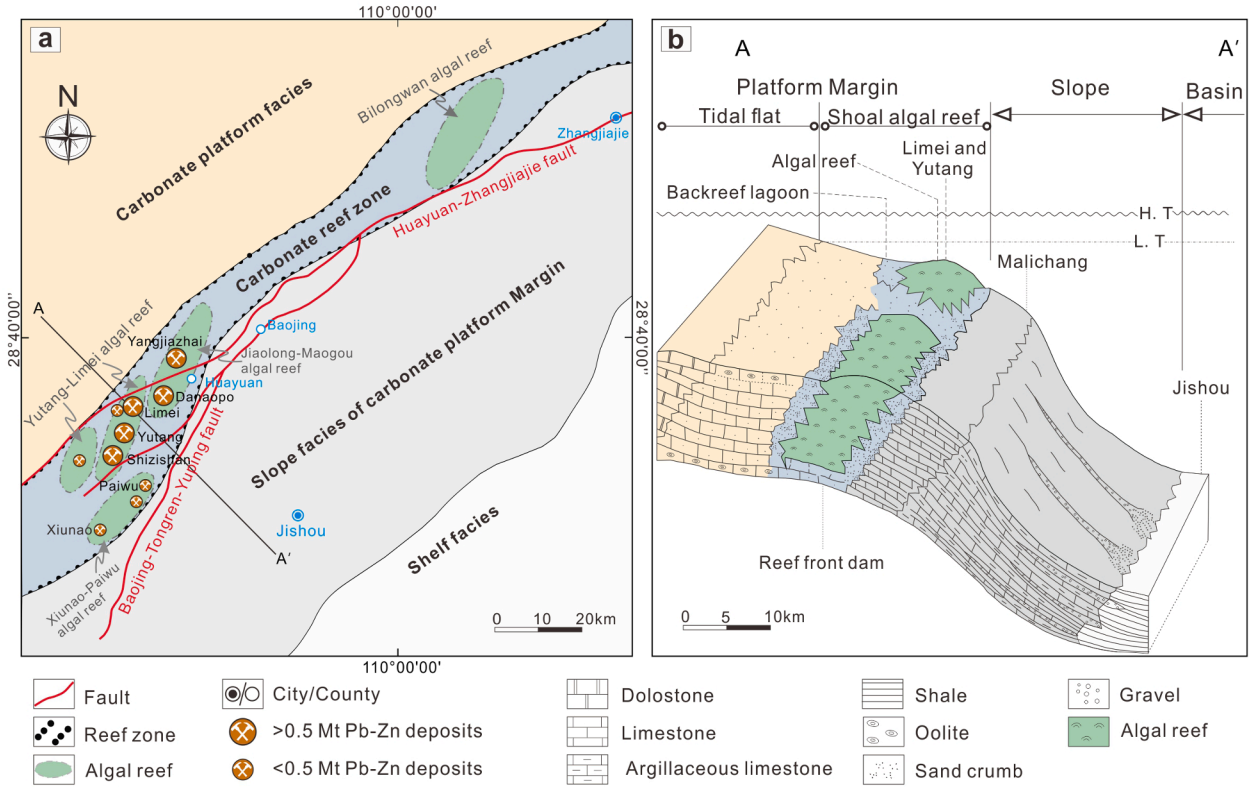

Fig. 2. (a) Sketch map of algal reef facies and paleogeographic environment in the Xiangxi–Qiandong area. (modified after Chen et al., 2018), (b) Cross-section A-A′ showing the location of the Limei and Yutang deposits, faults and sedimentary facies.

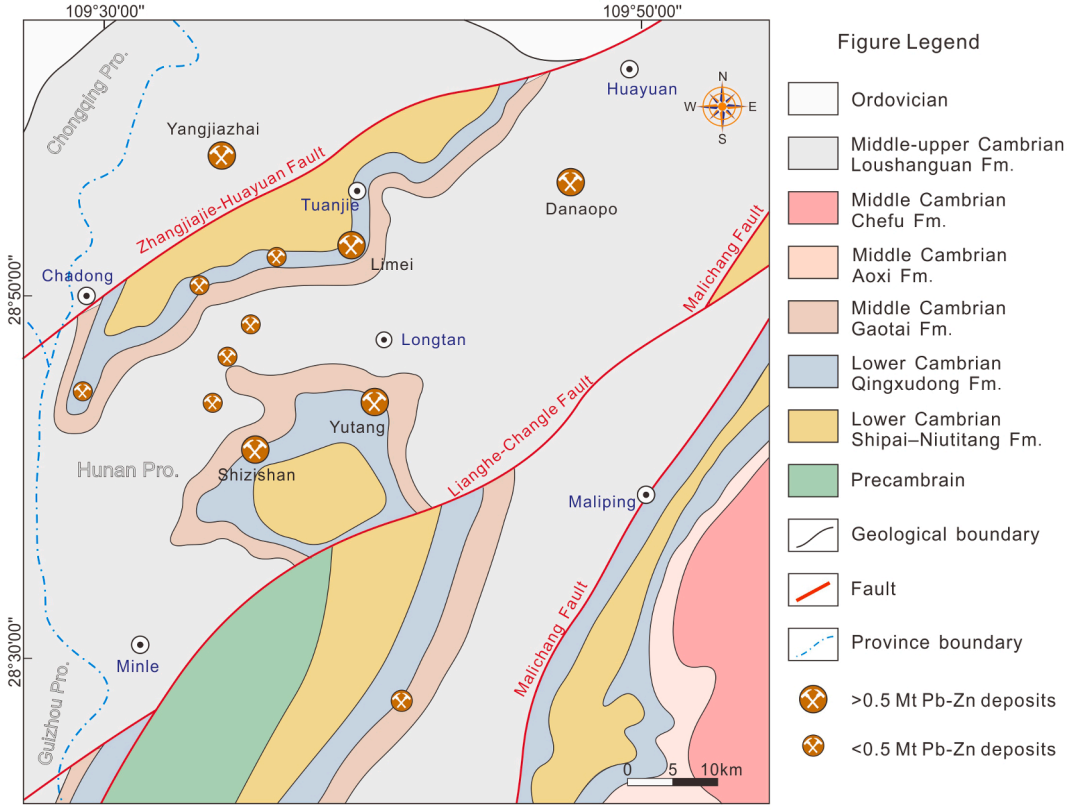

Fig. 3. Geological map of the Huayuan orefield showing the distribution of Pb-Zn deposits, sedimentary strata and faults (modified from Duan, 2014).

Yangjiazhai deposits, have been discovered in this orefield (Figs. 2–3), containing > 12.0 Mt Pb + Zn metal reserve with an average ore grade of ~ 4.0 wt% Pb + Zn.

Exposed strata at Huayuan comprises the metamorphosed basement made of the Banxi Group (Gp.) sandstone–siltstone and silty slate, the Late Ediacaran Dengying Fm. siliceous dolostone and the clastic and carbonate rocks of Lower–middle Cambrian to Ordovician strata. Regional dominantly NE- and ENE-trending faults include the Baojing-Tongren-Yuping (its northern segment is also known as the Malichang fault), the Songtao-Zhangjiajie (its northern segment known as the Huayuan-Zhangjiajie) and the Lianghe-Changle fault (Fig. 3). Among these structures, the Huayuan-Zhangjiajie fault controls the Pb-Zn mineralization in the orefield. Igneous rocks are absent in drill-holes and none are indicated by geophysical data (Du, 2014)

The Pb-Zn sulfide ores occur in reef zones of carbonate platform facies, particularly the reef limestone of the Lower Cambrian Qingxudong Fm. (Fig. 2; Tang et al., 2012). Drilling, trenching and test shafts show that the thickness of reef limestone positively correlates with mineralization intensity (Wei et al., 2017; Chen et al., 2018). The thickest sulfide orebodies were discovered in the core of the reef facies.

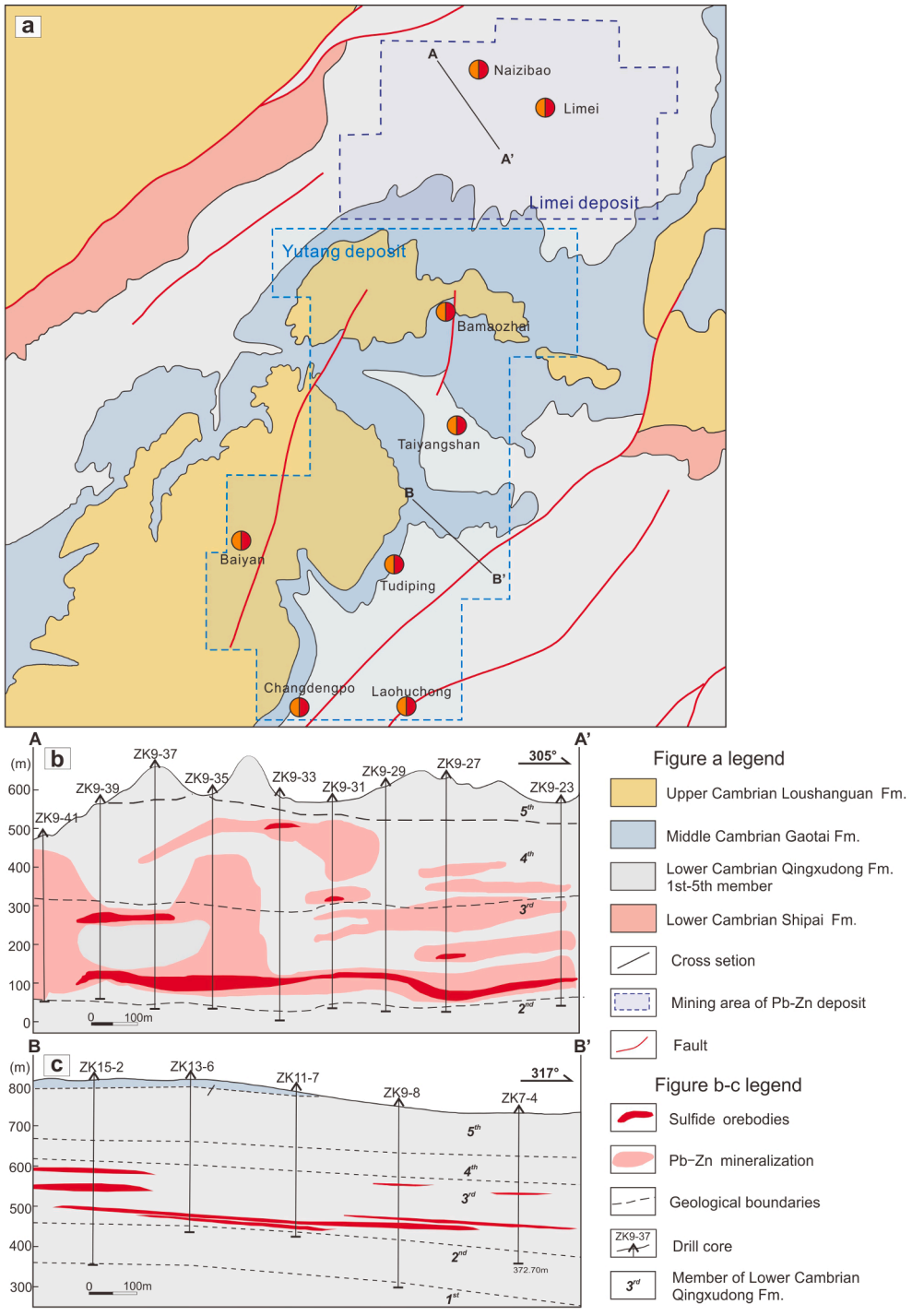

Fig. 4. (a) The geological map of Limei and Yutang Pb-Zn deposits. (b) Cross-section A–A′ of the Limei deposit showing the distribution of the sulfide ores. (c) Cross-section B–B′ of the Yutang deposit showing the occurrence of the sulfide ores.

2.3. The geology of the Limei and Yutang Pb-Zn deposits

At Limei and Yutang, the exposed strata are primarily of Lower to Middle Cambrian age (Fig. 4a and 5) and include (from bottom to top): (a) the argillaceous siltstone of the Lower Cambrian Shipai Fm., (b) Lower Cambrian Qingxudong Fm. consisting of limestone (lower part) and dolostone (upper part), (c) Middle Cambrian Gaotai Fm. argillaceous dolostone, and (d) argillaceous dolostone of the Upper Cambrian Loushanguan Fm. The Qingxudong Fm. is subdivided into five members, from bottom to top: (i) 1st member, dark-gray thin- to medium-bedded argillaceous zebra limestone, (ii) 2nd member consisting of gray/grayish-green medium- to thick-bedded intraclastic sandy-micritic limestone, (iii) gray-white thick-bedded algal reef limestone and clastic algal limestone (main ore host) of the 3rd member, (iv) 4th member, gray-white thick-bedded oolitic limestone and clastic limestone (the secondary ore host), and (v) 5th member, gray-white thick-bedded muddy-sandy dolostone and laminated dolostone.

2.3.1. Sulfide mineralization

Sulfide mineralization at Limei and Yutang occur as lenticular lenses and steeply irregular veins within the 3rd member of Qingxudong Fm. and to a lesser extent in the 4th member of Qingxudong Fm. (Figs. 4–5). At Limei, there are two contiguous mining zones, namely Limei and Naizibao (Fig. 4a). Currently, 10 orebodies have been found, containing

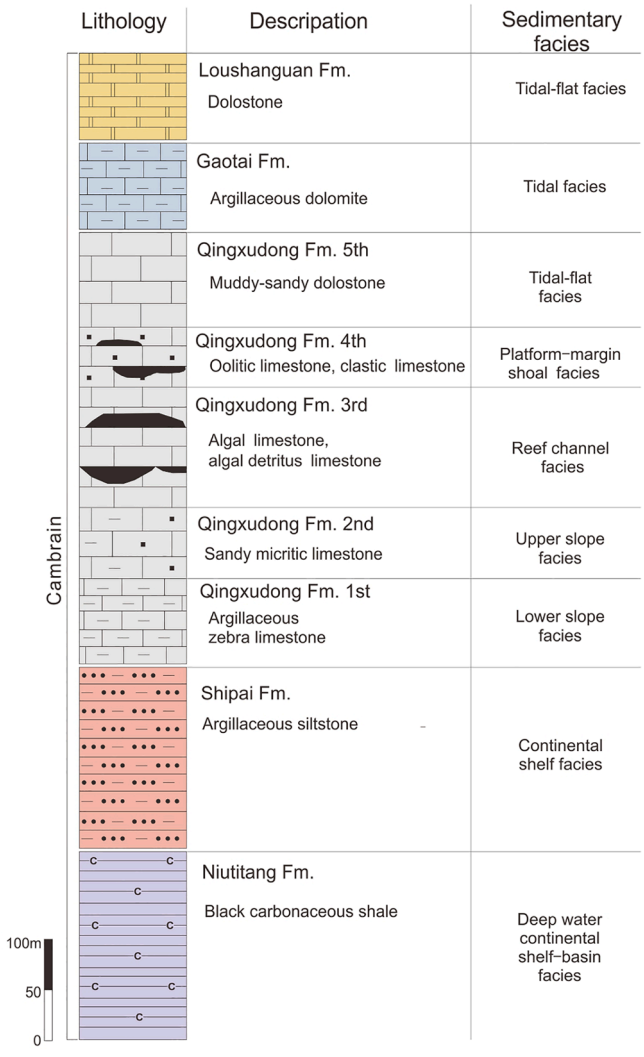

Fig. 5. Stratigraphic column of the Limei and Yutang mining areas, which shows the lithologies and location of the sulfide orebodies.

> 40.0 Mt ore at ~ 3.7 wt% Pb + Zn (Wei, 2017). The lenticular orebodies are usually multilayered (commonly 3–7 layers), with individual layers 1–20 m thick, 500–800 m long and 100–350 m wide on average. The fl-20-a orebody, the largest orebody at Limei, is mainly hosted in the bottom part of the Lower Cambrian Qingxudong Fm. 3rd member (reef limestone). The orebody is ~ 1500 m long, ~150 m wide and ~ 6 m thick and contains > 0.13 Mt Pb + Zn reserve with an average ore grade of 3.48 wt% Zn and 0.22 wt% Pb (Fu, 2011; Fig. 4b). The vein-type orebodies are strictly controlled by NE-trending faults. The individual vein is typically 5–50 cm wide and ~ 100 m long along strike with ore grades of 10–50 wt% Pb + Zn.

At Yutang, five contiguous mining zones including Bamaozhai, Taiyangshan, Tudiping, Changdengpo, Laohuchong and Baiyan are currently being mined with proven sulfide ores of > 130 Mt at an average ore grade of 4.68 wt% Pb + Zn. Two types of orebodies were recognized: (i) breccias interpreted to be of paleokarst-filled origin; the orebody in the 5th mining area of the Tudiping zone is 80 m long, 20 m wide and 10 m thick with a total Pb + Zn grade > 25%; (ii) stratiform replacement orebody, is widely distributed in the all mining zone of Yutang, account for 80% of the total Pb + Zn reserve (Fig. 4c).

2.3.2. Hydrothermal alteration

Wall-rock alteration at Limei and Yutang introduced calcite, organic matter, and fluorite with minor dolomite (Fig. 6). Calcite- and fluorite-altered zones are the most common. Calcite occurred widely in the Cambrian Qingxudong Fm. shows a close spatial relationship with the Pb-Zn mineralization (Fig. 6a, d–g, i–j). The presence of fluorite with sulfides was identified in this study, particularly in the 3rd member of the Cambrian Qingxudong Fm. In some cases, organic matter shows an intimate association with high grade sulfide ores (Fig. 6b,k).

2.3.3. Mineralogy and paragenesis

The ore mineralogy of Limei and Yutang shows little variation and mainly consists of sphalerite, galena and minor pyrite, accompanied by calcite, hydrothermal dolomite, fluorite and barite as the main gangue minerals (Figs. 6–7). Notably, a small amount of organic matter has been observed in this study (Figs. 6b, k; 7c,i). The main sulfide ores from the deposits occur as metasomatic replacements of carbonate rocks and open-space fillings. Disseminated sulfide ores are common in the stratiform replacement orebodies where sulfides occur as speckles and coalesce to form aggregates in the host rocks or calcite/ hydrothermal dolomite (Figs. 6a, d–l, 7j, i). High-grade orebodies fill open spaces such as veins (Fig. 6a, f, g), solution-collapse breccias (Fig. 6d, i, j, k) and massive (Fig. 6c).

Limei

The paragenetic sequence for Limei was established from the morphology, texture and mineral assemblages (Figs. 6–7). Three separate hydrothermal events can be distinguished (Fig. 8). Sulfides were mainly precipitated in ore stages 1 and 2.

Stage 1(S1)

Euhedral pyrite (termed Py1), the earliest hydrothermal mineral in the entire ore-forming process, is medium to coarse-grained (200–1000 μm in diameter) and is very abundant (Fig. 7a). Porous sphalerite (termed Sp1) accompanies Py1 as coarse-grained (0.5–1.0 cm in diameter). Commonly, Sp1 enclosed or replaced early Py1 (Fig. 7a,c). In some cases, calcite overgrows on Sp1 and/or cuts early formed sulfides (Fig. 7a-b). Locally, minor galena 1 (termed Gn1) is replaced by later sphalerite (termed Sp2) (Fig. 7b).

Stage 2 (S2)

Sp2 and coeval galena (termed Gn2) are the main mineral assemblages in Stage 2. Sp2 commonly is corroded by later coarse-grained Gn2 (Fig. 7c). In some cases, Sp2 partially dissolves and replaces the early formed Gn1 (Fig. 7b). Gn2 occurs as replacements or overgrowths on early ore-stage sulfides (Sp1 and Py1; Fig. 7c). Commonly, calcite, organic matter and hydrothermal dolomite fill vugs or cracks in sulfide minerals (Fig. 7b–c, f. Locally, sparse fine-grained (<10 μm in diameter)

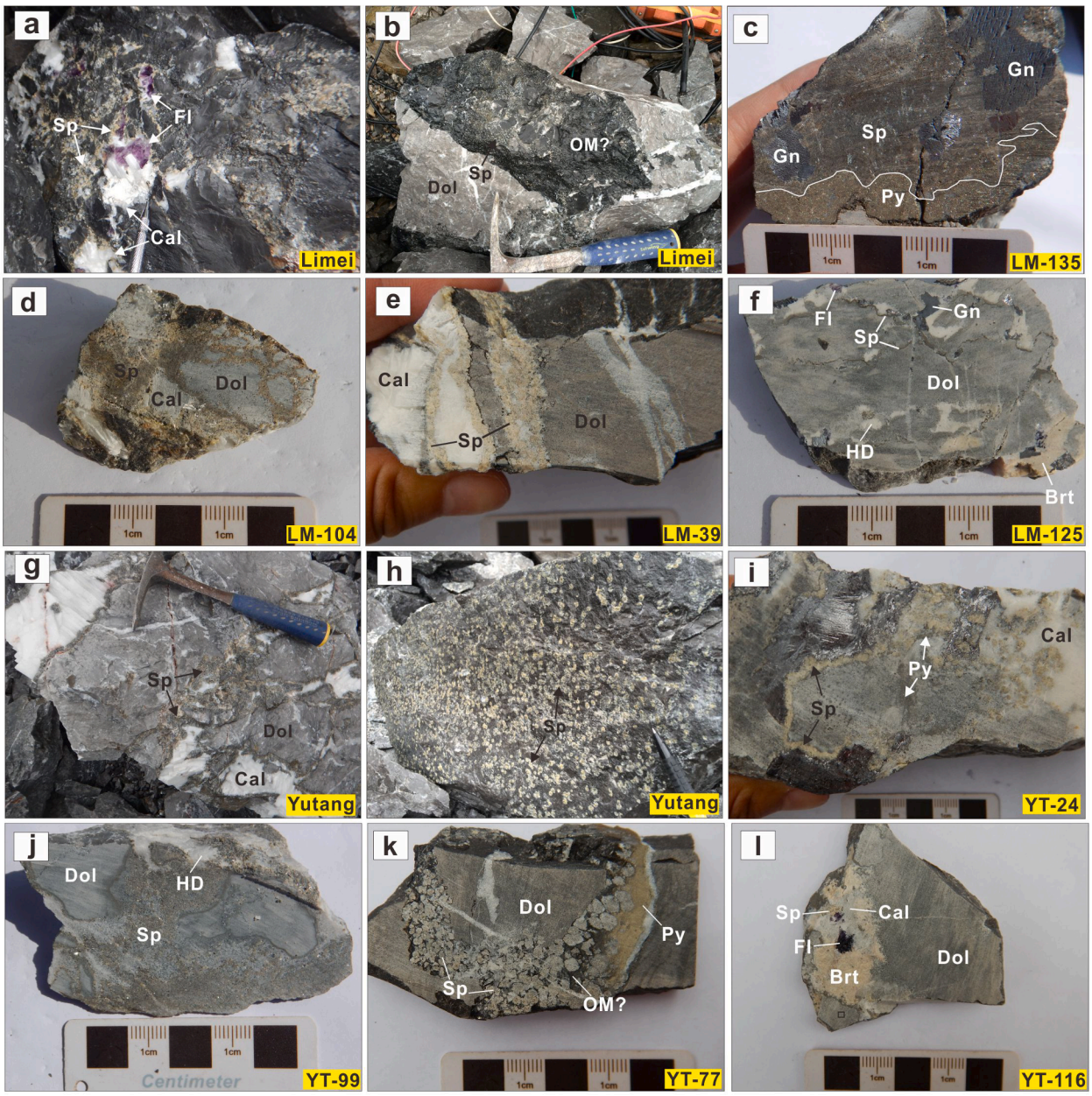

Fig. 6. Photographs of field and hand-specimens from the Limei (a-f) and Yutang (g-l) deposits. (a) Sphalerite, fluorite and calcite cement the carbonate breccias. (b) Sulfide-bearing organic matter in the fracture of carbonate rocks. (c) Massive sulfide ore. (d) Breccia-hosted sulfide with calcite cement. (e) Banded sphalerite ore within the fracture of the host rocks. (f) Disseminated sulfide ore filled in the dissolved voids of the host rocks. (g) Stockwork sulfides cement the carbonate breccias. (h) Dense disseminated sphalerite in the interface of host rocks. (i) Pyrite-sphalerite-galena mineral assemblage. (j) Sulfide ore replacing and/or dissolving the host rocks. (k) coarse-grain sphalerite aggregates filled in the vug of the host rocks. (l) Sphalerite, calcite and fluorite overgrowth with barite. Mineral abbreviations: Py = pyrite, Sp = sphalerite, Gn = galena, HD = hydrothermal dolomite, OM = organic matter, Fl = fluorite, Cal = calcite, Brt = barite, Dol = dolostone.

pyrite (termed Py3) aggregates are randomly distributed in vugs or cracks in the sulfide minerals (Fig. 7e).

Stage 3 (S3)

Stage 3 represents the deposition of hydrothermal dolomite, fluorite, calcite and barite, which are the last mineral assemblages formed. These minerals commonly fill vugs and/or fractures in previously described sulfide minerals (Fig. 7c–d, f).

Yutang

The hydrothermal history at Yutang can be divided into are three stages (S1–3): early ore-stage S1, main ore-stage S2 and late ore-stage S3 (Fig. 8).

S1

The early ore S1 consists of abundant euhedral pyrite (termed Py1) and porous sphalerite (termed Sp1), accompanied by minor calcite as the main gangue mineral. These sulfides are primarily euhedral- to subhedral-grains. Py1 is fine- to coarse-grained (50–1000 μm in diameter) and commonly replaced or enclosed by Sp1 (Fig. 7g–h). Alternatively, Sp1 is subhedral coarse-grained (500–1000 μm in diameter) and commonly replaced by later galena (termed Gn2) (Fig. 7g–h). Locally, organic matter and calcite fill in vugs and/or fractures in the early sulfides (Fig. 7i).

S2

The main ore S2 is characterized by abundant sphalerite (Sp2), coarse-grained (100–1000 μm in diameter) galena (Gn2) and minor fine-grained (<10 μm in diameter) pyrite aggregates. Sp2 is commonly replaced by later Gn2 (Fig. 7h) or enclosed by later Gn2 and Py2

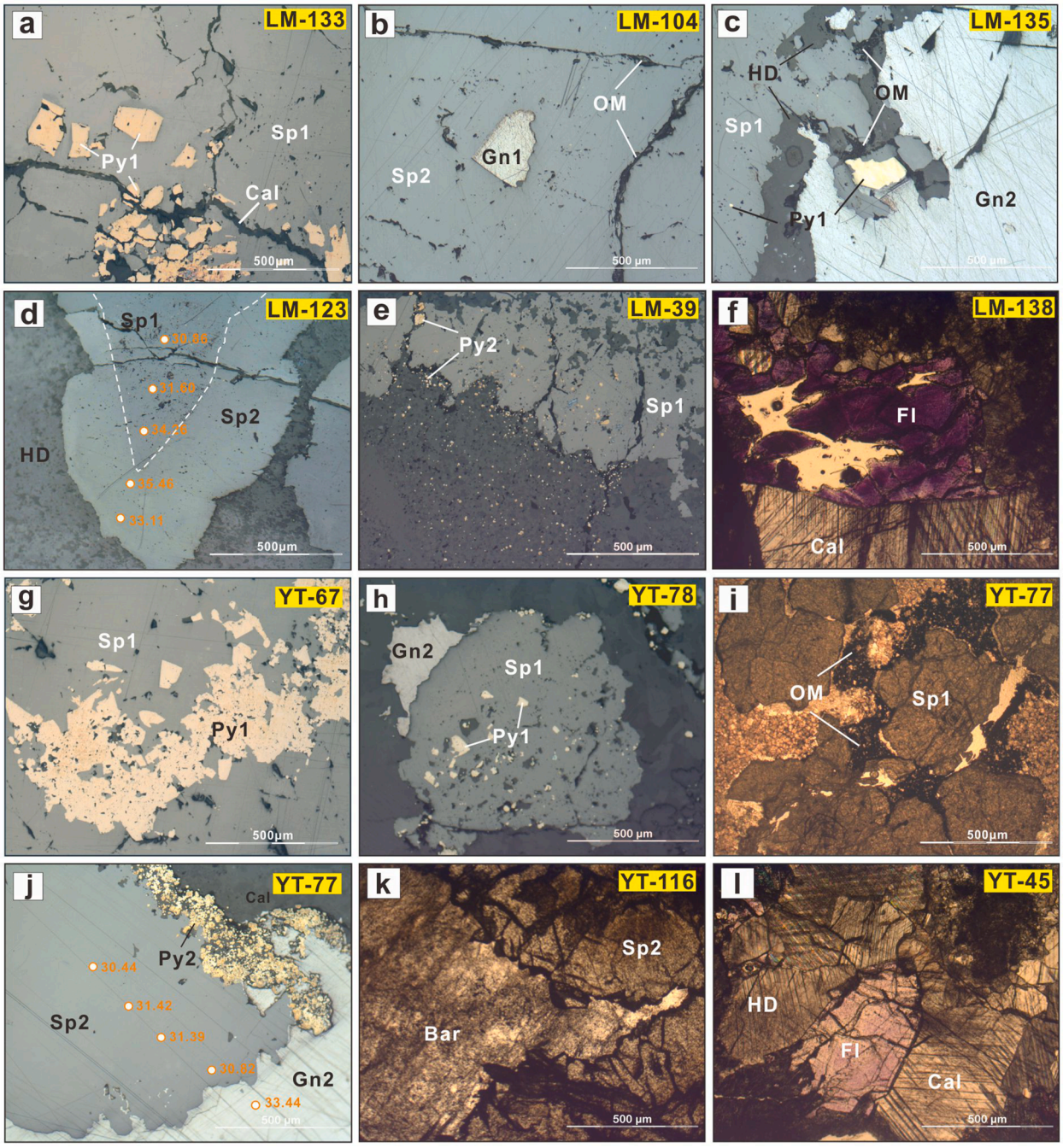

Fig. 7. Photomicrographs of ore textures of hydrothermal minerals in the Limei (a-f) and Yutang (g-l) deposits, with sulfur isotope data of reprehensive sulfide grains. (a) Euhedral Py1 enclosed and/or dissolved by Sp1. (b) Gn1 enclosed and/or replaced by Sp2, cut by later OM-bearing calcite veins. (c) Hydrothermal dolomite filled in the vug of early sulfide assemblages. (d) Coarse-grained sphalerite crystal showing clear boundary between Sp1 and Sp2. (e) Fine-grained Py2 filling fractures of inclusion-bearing Sp1. (f) Purple fluorite and calcite in vugs the host rocks. (g) Py1 enclosed and/or replaced Sp1. (h) Pyrite (Py1)–sphalerite (Sp1) assemblages replaced by later Gn2. (i) Calcite and organic matter filled in Coarse-grained Sp1. (j) Sp2 partially replaced by Gn2 and fine-grained Py2 aggregates distributed along their crystal boundaries. (k) Later formed barite fill in the vugs of Sp2. (l) Euhedral fluorite overgrowth with hydrothermal dolomite and calcite. Mineral abbreviations are the same as in Fig. 6. (For interpretation of the references to color in this figure legend, the reader is referred to the web version of this article.)

(Fig. 7j). Gn2 replaces or overgrows early sulfides (Fig. 7h, j). Locally, Py2 aggregates are irregularly distributed along the margin of early sulfides (Fig. 7j).

S3

During stage 3 (S3), gauge minerals such as calcite, hydrothermal dolomite, barite and fluorite were deposited in vugs, representing the last paragenetic stage (Fig. 7h–l). These minerals commonly occur as subhedral to euhedral grains and fill in the residual porosity of the early formed sulfides.

3. Sampling and analytical methods

3.1. Sampling

More than 200 samples are systematically collected from several mining levels at Limei and Yutang during field investigation. Among them, nine fluorite samples were prepared under a binocular microscope by use of micro-drill or handpicking for trace elements analysis, and twenty-seven representative sulfides covering the main hydrothermal

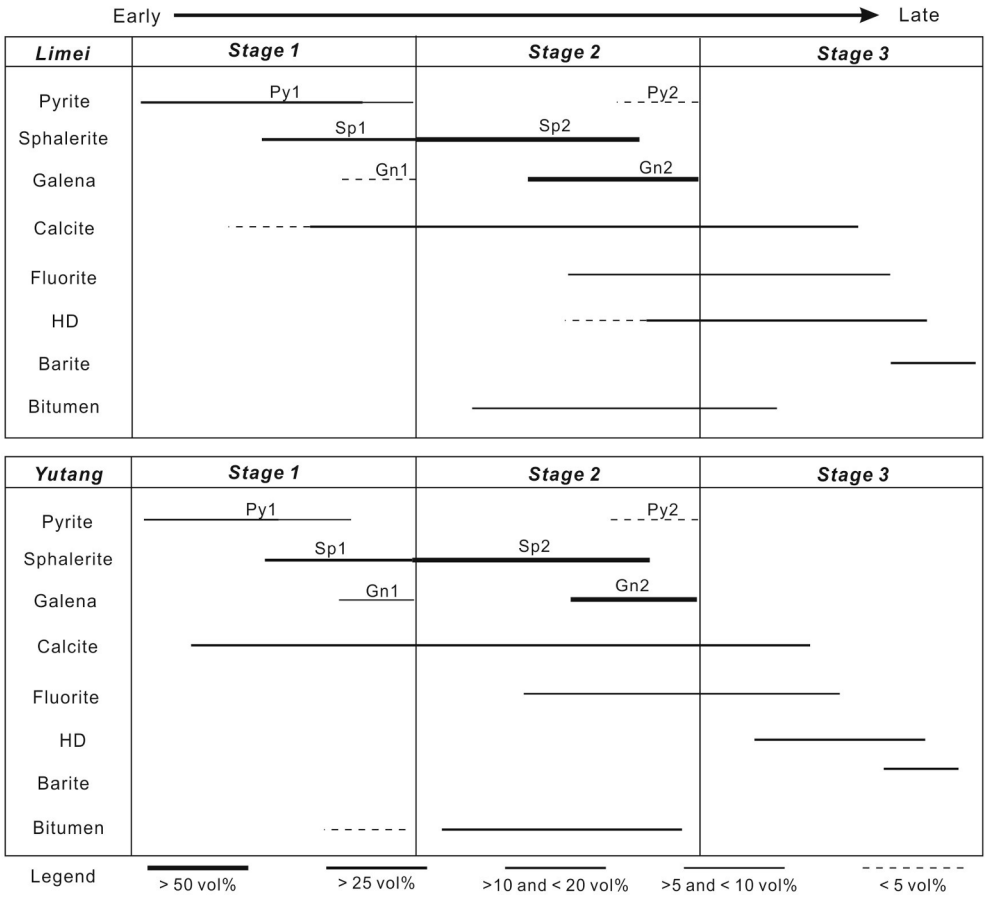

Fig. 8. Mineral assemblages and paragenetic sequences of the Limei and Yutang deposits, Huayuan district.

stages were collected for in situ S and Pb isotope analysis.

3.2. Analytical methods

3.2.1. Bulk REY analysis

The contents of REY were analyzed by ELAN DRC-e Q-ICPMS (PerkinElmer, Canada) at the State Key Laboratory of Ore Deposit Geochemistry, Institute of Geochemistry Chinese Academy of Sciences (IGCAS). The analytical procedure is described by Qi et al. (2000). The trace element (incl. REY) analysis of fluorite comprises the following steps: (i) 50 mg of powder samples were dissolved in a Teflon bomb using 1 mL HF and 0.5 mL HNO_3; (ii) the sealed bomb was placed on a hot plate, and the solution was evaporated to dryness to remove most of the silica; (ii) 1 mL HNO_3 was added. The sealed bombs were then placed in an electric oven and heated to 190 °C for 24 h; (iv) after cooling, 200 ng Rh was added as the internal standard and the solution was then dried down; (v) 2 mL of HNO_3 was added, evaporated to dryness and followed by a second addition of HNO_3 and evaporation to dryness; (vi) the final residue was re-dissolved in 2 mL HNO_3, resealing the bombs and returning them to heat in an electric oven at 140 °C for 5 h. The final solution was diluted to 100 mL by the addition of distilled de-ionized water for ICPMS analysis. The analytical precision is better than 10% (Qi et al. 2000).

3.2.2. In situ S and Pb isotope analysis

S isotopes were analyzed at the State Key Laboratory of Continental Dynamics, Northwest University, China, using Nu-Plasma 1700 MC-ICPMS system (Nu Instruments, UK) combined with a Resolution M-50 laser ablation system (ASI, Australia) equipped with a 193 nm ArF excimer laser (Coherent, USA). Details of the analytical method can be found in Chen et al. (2017). Sulfides (pyrite, sphalerite and galena) were ablated at a spot size of 30 μm, using a fluence of 3.6 J/cm^2 at 3 Hz. The total S signal obtained for sphalerite was typically 8 to 12 V. Under these conditions, after a 30 s background collection, 50 s of ablation signal collection is needed to obtain an internal precision of $^{34}S/^{32}S \leq \pm 0.000002$ (1σ). Instrument drift and mass bias were corrected using a sample standard bracketing (SSB) approach with repeated measurement of the standard before and after each sample. The international standard, NBS123 (sphalerite) and in-house standards Py-4 (pyrite) and CBI-3 (galena) were used for calibration in the sulfur isotope analyses. The analytical precision calculated from replicate analyses of unknown samples is better than 0.1‰ (1σ). The measured $\delta^{34}S_{CDT}$ (‰) of 17.8 ± 0.5‰ (2σ, n = 156) for standard NBS123 agrees well with that of the reported value of 17.8 ± 0.2‰ (Chen et al., 2017).

Using the same laser ablation system as in the S isotope spot analysis, in situ Pb isotopes were analyzed using Nu-Plasma II MC-ICPMS system (Nu Instruments, UK), following a method reported previously by Bao et al. (2016). Samples were ablated with a spot size of 9 μm for galena and 100 μm for sphalerite and pyrite with a laser ablation frequency of 3.0 J/cm^2 at 4 Hz. Each sample acquisition consisted of a background measurement time of 30 s followed by 50 s of ablation for signal collection and an additional 40 s of wash time to reduce memory effects. To ensure the same ^{208}Pb signals were obtained from different samples with disparate Pb concentrations, The Tl NIST SRM 997 (20 ppb, $^{205}Tl/^{203}Tl$ = 2.38890) and NIST SRM 610 glass were used as internal and external Pb isotope standards, respectively. The average Pb isotopic compositions of NIST SRM 610 in this study are 17.050 ± 0.004 for $^{206}Pb/^{204}Pb$, 15.510 ± 0.002 for $^{207}Pb/^{204}Pb$ and 36.985 ± 0.006 (1σ) for $^{208}Pb/^{204}Pb$, consistent with the reported reference ratios (Bao et al., 2016).

4. Results

4.1. REY in fluorite

The complete ICPMS data set for REY in fluorite is provided in Table 2 and the data normalized to chondrite (Sun and McDonough, 1989) are presented in Fig. 9a. Despite the color and textural variations between two generations of fluorite, both show a broadly similar REY pattern. Bulk fluorite at Limei and Yutang have low REY contents (0.47 to 8.67 ppm; mean, 3.99 ppm, Table 2 relative to that from the North Pennine Orefield, England (Bau et al., 2003). These fluorite are slightly depleted in LREE and HREE relative to MREE, resulting in slight convex-upward shaped REE patterns (Fig. 9a). They also exhibit a weak negative Ce_{SN} but strong positive Eu_{SN} anomalies in fluorite. The ratios of La/Ho and Y/Ho are ranging from 22.0 to 120 (mean = 65.3) and 61.0 to 176 (mean = 133) (Fig. 9b).

4.2. Sulfur isotopic compositions

The range and distribution of $\delta^{34}S$ values of sulfides from Limei and Yutang are presented in Appendix Table 1 and shown in Figs. 10–11. In situ $\delta^{34}S$ values of sulfides (pyrite, sphalerite and galena) from Limei and Yutang range from + 27.66 to + 35.46‰ (mean, +32.23‰) and + 24.80 to + 36.07‰ (mean, +32.69‰), respectively, in agreement with the previous bulk S isotopic data from Limei (Cai et al., 2014; Zhou et al., 2016; Wei et al., 2017) and Yutang (Wei et al., 2017; Li et al., 2017). Interestingly, there is variation in the sulfide isotopic composition within single grain of most sulfides (Fig. 7d, j). For example, the $\delta^{34}S$ values of a sphalerite grain from sample LM-123 (Limei; Fig. 7d) vary from + 30.86 to + 35.46‰.

At Limei, the $\delta^{34}S$ values were different among the sulfides from stages 1 and 2 (Fig. 10). Specifically, Gn2 has the lowest $\delta^{34}S$ values (+29.67 ± 0.14‰, n = 4), followed by Py1 (+31.55 ± 1.09‰, n = 7), Sp1 (+32.74 ± 1.12‰, n = 22) and Sp2 (+32.74 ± 1.48‰, n = 16). By contrast, Sp1 and Sp2 at Yutang have similar $\delta^{34}S$ values (+30.82 to + 35.90‰ and + 30.44 to + 36.07‰, respectively) with average values of + 33.44 ± 1.70‰ (n = 8) and 33.71 ± 1.85‰ (n = 10). Followed by Py1, its $\delta^{34}S$ values shows significantly variable, ranging from + 24.80 to + 33.10 ‰ (+29.06 ± 3.85‰, n = 4). In addition, two spots of Gn2 (in S2) yielded $\delta^{34}S$ values from + 30.11 to + 33.44‰ (+31.78 ± 1.66‰).

4.3. In situ Pb isotope ratios

In situ Pb isotope ratios of sulfides from Limei and Yutang are presented in Appendix Table 2 and shown in Fig. 12. Sulfide minerals (pyrite, sphalerite and galena) from Limei and Yutang show relatively narrow ranges in Pb isotope ratios as follows: $^{206}Pb/^{204}Pb$ (18.001 to 18.384), $^{207}Pb/^{204}Pb$ (15.645 to 15.924) and $^{208}Pb/^{204}Pb$ (38.243 to 38.874), consistent with the previous bulk Pb isotope ratios (see Fig. 12a-b; data from Cai et al., 2014; Zhou et al., 2016; Wei et al., 2017). Sulfide minerals analyzed from Yutang have relatively larger ranges of $^{206}Pb/^{204}Pb$ (18.135–18.384), $^{207}Pb/^{204}Pb$ (15.714–15.924) and $^{208}Pb/^{204}Pb$ (38.347–38.874) relative to that of Limei ($^{206}Pb/^{204}Pb$ = 18.001–18.269, $^{207}Pb/^{204}Pb$ = 15.645–15.796 and $^{208}Pb/^{204}Pb$ = 38.243–38.597). Furthermore, positive correlations between $^{207}Pb/^{204}Pb$ and $^{206}Pb/^{204}Pb$ and between $^{208}Pb/^{204}Pb$ and $^{206}Pb/^{204}Pb$ were observed for all investigated samples (Fig. 12a-d).

At Limei and Yutang, Pb isotope ratios show significant differences between the sulfides from two ore stages (Fig. 12c-d. Specifically, sulfides at S1 from Limei and Yutang have less radiogenic Pb isotope ratios relative to that of S2.

Table 2
The rare earth elements and yttrium (REY) contents (ppm) for fluorite separate from the Limei and Yutang deposits in the Huayuan district.

Sample No.	Location	Color	La	Ce	Pr	Nd	Sm	Eu	Gd	Tb	Dy	Y	Ho	Er	Tm	Yb	Lu
Limei																	
LM17-138	Naizibao	Purple	0.964	0.088	0.012	0.417	0.242	4.957	0.800	0.003	0.011	1.340	0.008	0.016	0.001	0.004	0.004
LM17-130	Naizibao	White	0.157	0.096	0.013	0.059	0.050	0.602	0.105	0.002	0.016	0.563	0.004	0.008	0.001	0.009	0.002
LM17-35	Naizibao	Purple	0.953	0.051	0.005	0.408	0.223	5.069	0.813	0.003	0.021	1.260	0.008	0.007	0.001	0.002	0.005
LM17-41	Limei	Purple	0.760	0.380	0.039	0.402	0.174	2.713	0.437	0.005	0.014	1.130	0.009	0.019	0.002	0.008	0.009
LM17-48	Limei	White	0.133	0.188	0.022	0.068	0.005	0.147	0.036	0.002	0.010	0.244	0.004	0.005	0.001	0.010	0.002
Yutang																	
YT17-35	Tudiping	Purple	0.268	0.284	0.026	0.128	0.049	0.650	0.102	0.003	0.056	1.280	0.008	0.007	0.001	0.007	0.004
YT17-4	Babaozhai	Purple	0.312	0.372	0.038	0.191	0.042	0.903	0.139	0.008	0.047	0.597	0.006	0.019	0.002	0.018	0.004
YT17-149	Tudiping	White	0.333	0.078	0.007	0.155	0.113	1.733	0.311	0.003	0.009	0.705	0.004	0.009	0.001	0.006	0.002
YT17-51	Changdengpo	White	0.044	0.059	0.008	0.016	0.007	0.065	0.017	0.002	0.009	0.214	0.002	0.011	0.001	0.008	0.003

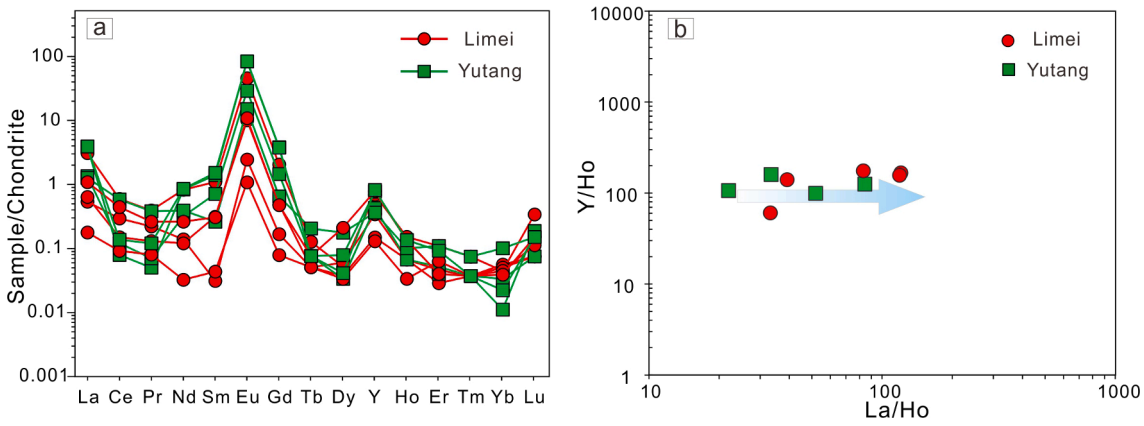

Fig. 9. (a) Chondrite-normalized REY (REY_{SN}) distribution patterns of fluorite samples from Limei and Yutang. Data are normalized to chondrite (Sun and McDonough, 1989). (b) La/Ho vs Y/Ho for fluorite from the Limei and Yutang deposit (modified after Bau and Dulski, 1995).

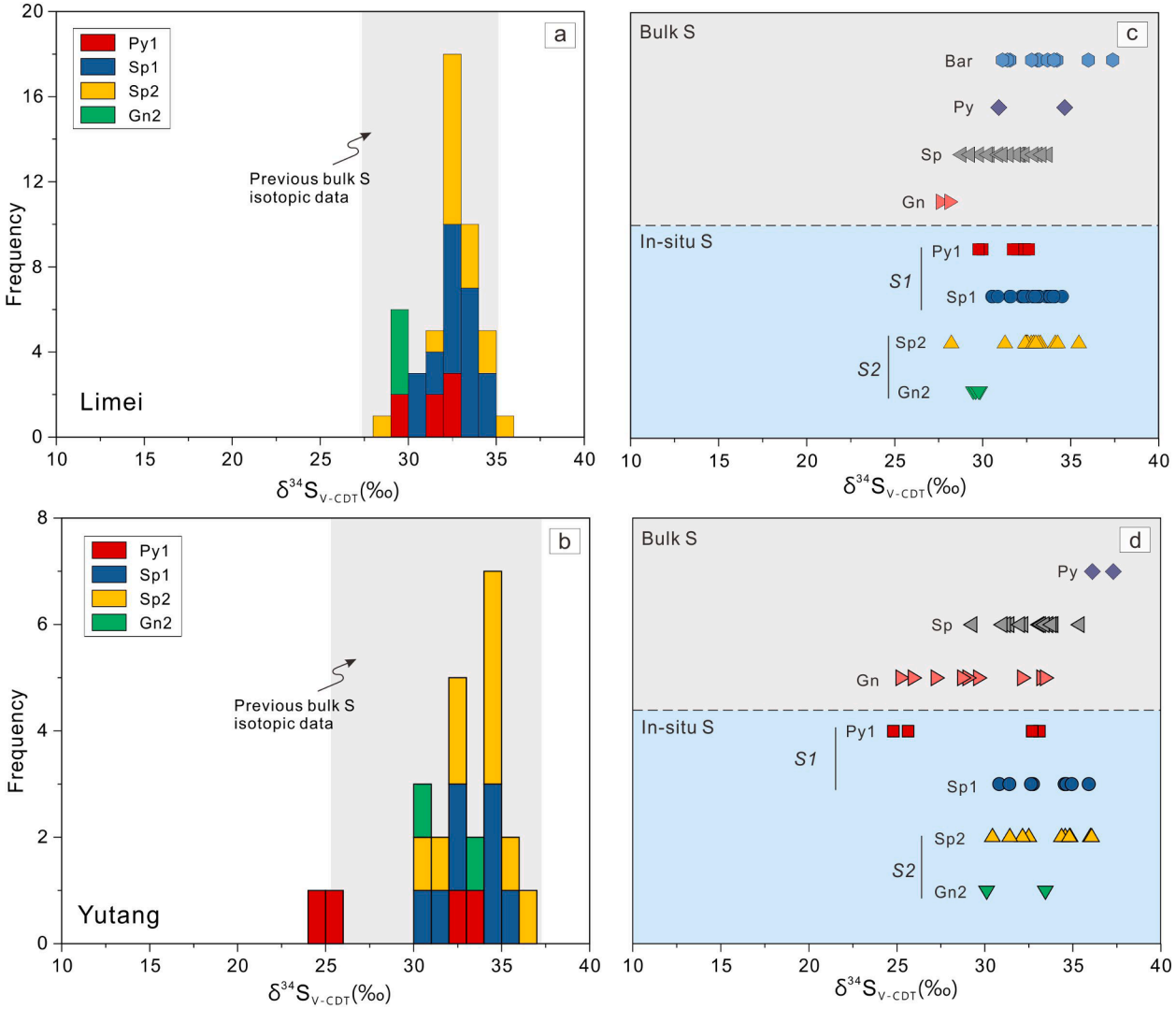

Fig. 10. A histogram of $\delta^{34}S$ values for various ore minerals from different ore stages of Limei (a) and Yutang (b). Distribution of in situ $\delta^{34}S$ values of sulfides from different ore stage at Limei (c) and Yutang (d) compared to those previously reported bulk $\delta^{34}S$ values (data from Cai et al., 2014; Zhou et al., 2016; Li et al., 2017; Wei et al., 2017).

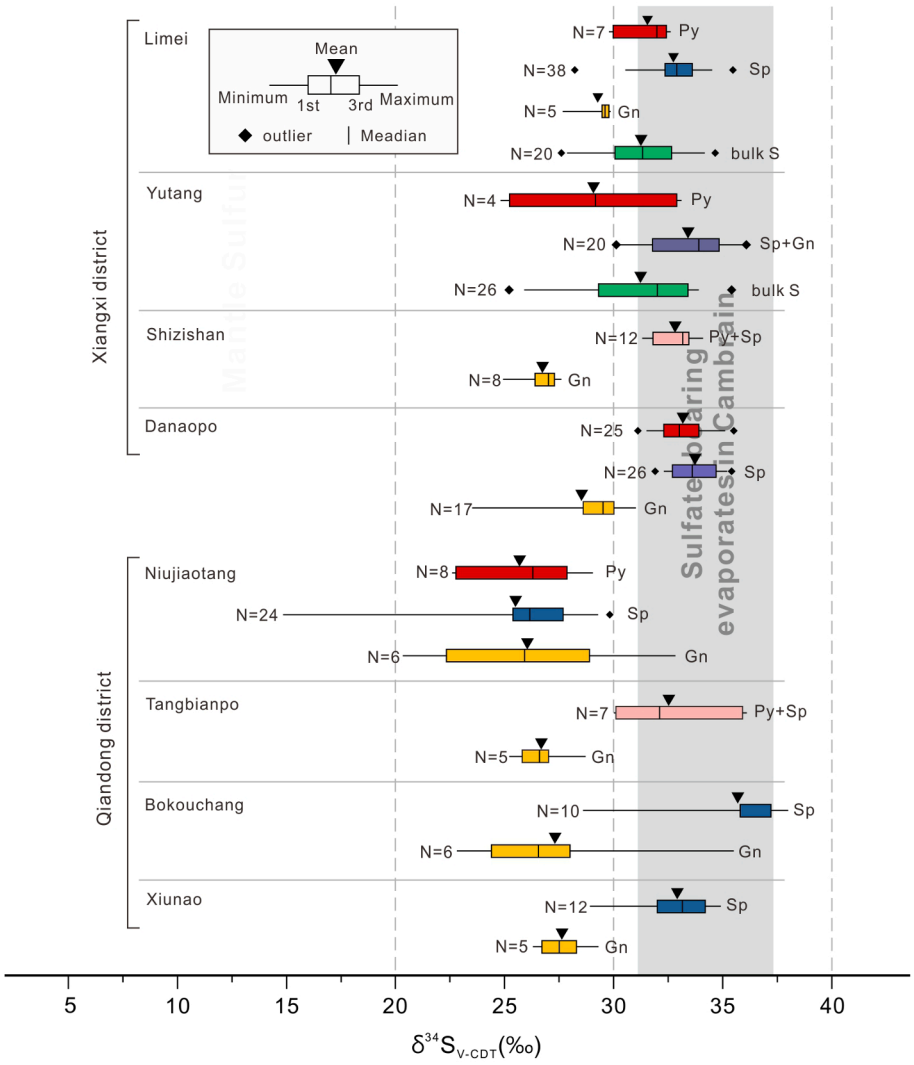

Fig. 11. Compilation of $\delta^{34}S$ values for sulfides from the early Cambrian carbonate-hosted Pb-Zn deposits from the XQMB, including Limei (data from Cai et al., 2014; Zhou et al., 2016; Wei et al., 2017 and this study), Yutang (data from Li et al., 2017, Wei et al., 2017 and this study), Shizishan (Duan, 2014) Danaopo (data from Wu et al., 2021), Niujiaotang (data from Ye et al., 2005, 2012), Tangbianpo (data from Yu et al., 2017), Bokouchang (data from Cai et al., 2014) and Xiunao (data from Cai et al., 2014; Li, 2018) deposits. The $\delta^{34}S$ values of sulfides were analyzed using both bulk and in situ techniques.

5. Discussion

5.1. Constraints from REY in fluorite

REY geochemistry has a significant potential for deciphering the ore-forming process and elements sources (Bau and Dulski, 1995; Souissi et al., 2007; Zou et al., 2017, Zou et al., 2020). In this study, fluorite is spatially associated with the ore-stage sulfides (Fig. 6a,f,l). As shown in Fig. 9a, REY patterns of fluorite from Limei and Yutang are similar in terms of MREE-enrichment and Eu_{SN} anomalies, indicating that the Limei and Yutang share a similar source for ore-forming elements (Fang et al., 2020; Zou et al., 2022). Moreover, fluorite samples from Limei and Yutang display a relatively narrow Y/Ho ratio (61.0–176) and are close to a straight line on a Y/Ho versus La/Ho diagram (Fig. 9b), indicating that the ore-forming fluids of Limei and Yutang are originated from the same fluid system (Bau and Dulski, 1995)

The Eu and Ce anomalies of Ca-bearing minerals are indicators of the ore-forming fluid temperature and redox conditions (Bau and Dulski, 1995; Souissi et al., 2007). All fluorite from Limei and Yutang has recognizable Ce_{SN} anomalies, which are comparable to that of MVT deposits worldwide (e.g., Bau et al., 2003; Souissi et al., 2007). Whilst, strong positive Eu_{SN} anomalies in fluorite from Limei and Yutang are observed (Fig. 9a), which can be caused by two mechanisms: (i) in the low-temperature condition (<200 °C), a significant amount of Eu occur as Eu^{3+} (similar to the Ca^{2+} ionic radius), which facilitates substitution for Ca^{2+} in the fluorite structure and thus results in positive Eu anomalies (Bau and Dulski, 1995); (ii) they can be inherited from the source rock (including feldspar). Hydrothermal fluid with positive Eu anomalies due to the interaction with Eu^{3+}-rich minerals (Souissi et al., 2007). In contrast, the Huayuan orefield lacks such sedimentary rocks with significant positive Eu anomalies (Wei, 2017; Hu et al., 2020). Meanwhile, fluid inclusions data demonstrated the temperature of mineralizing fluid significantly is < 200 °C (Liu and Zheng, 2000). Therefore, the positive Eu anomalies of fluorite in the Limei and Yutang deposits indicate that the REEs signature could be inherited from the low-temperature parental fluid.

The enrichment of Gd and Tb may reflect the fact that REEs are transported as fluoride complexes because Tb and Gd are easily formed as stable complexes with F relative to other REEs. Given this assumption, the lack of a positive Tb and Gd anomaly in the Yutang and Limei fluorite indicates that fluoride complexes are unlikely to have been the main form of transport for REE. This finding is also supported by theoretical calculations by Migdisov et al. (2009). All REEs could be efficiently transported as chloride and sulfate complexes rather than fluoride complexes under hydrothermal conditions and at temperatures similar to those that prevailed in the Huayuan orefield (<200 °C) (Migdisov and Williams-Jones, 2007). At Limei and Yutang, the high contents of H_2S in fluid inclusions of hydrothermal calcite and sphalerite (e.g., Liu and Zheng, 2000) suggest sulfate complexes may be ruled out as the main transport. Conversely, the high salinity of the mineralizing

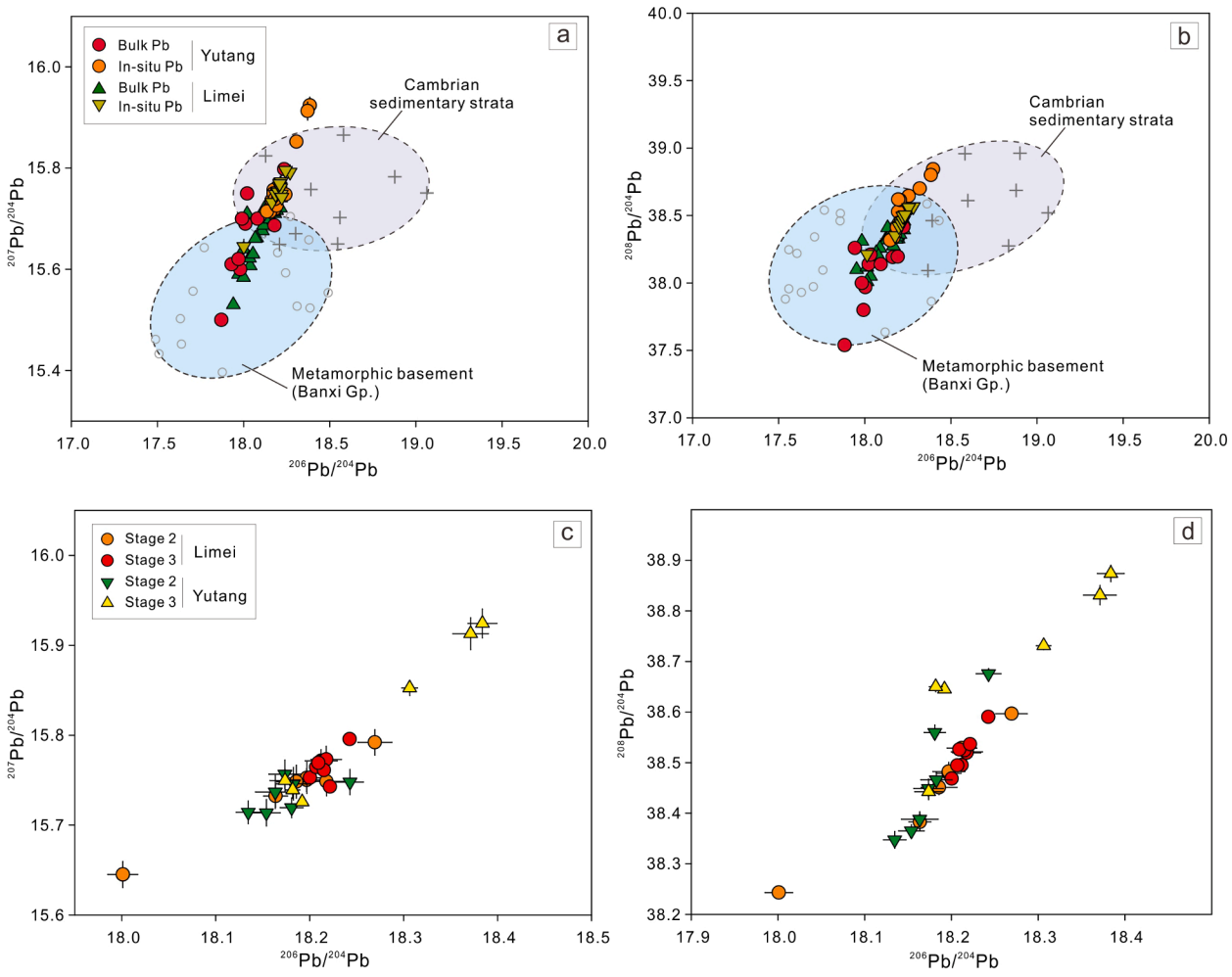

Fig. 12. Comparison plot of $^{206}Pb/^{204}Pb$ vs. $^{207}Pb/^{204}Pb$ (a) and $^{206}Pb/^{204}Pb$ vs. $^{208}Pb/^{204}Pb$ (b) for the Limei and Yutang Pb-Zn deposits, early Cambrian sedimentary strata and Proterozoic basement rocks; Binary plot of $^{206}Pb/^{204}Pb$ vs. $^{207}Pb/^{204}Pb$ (c) and $^{206}Pb/^{204}Pb$ vs. $^{208}Pb/^{204}Pb$ (d) for sulfide formed at S1–2 in the Limei and Yutang deposits. Bulk Pb isotope ratios in sulfides of Limei and Yutang deposits from Cai et al. (2014), Zhou et al. (2016), Wei et al. (2017). The Pb isotope data of Cambrian sedimentary strata and Proterozoic basement rocks from Schneider et al. (2002), Cai et al. (2014) and Hu et al. (2015).

fluids (avg. 22.7 ± 5.8 wt% NaCl eqv.; Liu and Zheng, 2000) and the occurrence of sylvite and halite daughter minerals (Liu et al. 1997) indicate that chloride was the dominant anion and that the REE distribution in the fluid was controlled mainly by chemical complexes rather than sorption of uncomplexed REE species. Furthermore, extremely high Cl^- concentrations in sphalerite fluid inclusions was determined by atomic absorption spectrometry (Liu and Zheng, 2000). Hence, REEs and by inference other metals likely transported with chloride complexes at Huayuan.

5.2. *Implications from sulfur isotopic compositions*

5.2.1. *Source of S*

In situ S isotopic data of sulfides from both Limei ($\delta^{34}S$= +27.66 to + 35.46‰) and Yutang ($\delta^{34}S$= +24.80 to + 36.07‰) are significantly higher than 15‰ (Figs. 10–11), reflecting $\delta^{34}S$-enriched hydrothermal fluids, a typical characteristic of marine sulfate isotopic signatures (Seal, 2006). In Limei and Yutang, the sulfide-bearing minerals are primarily sphalerite, galena, and pyrite but sulfate minerals (e.g., barite; Fig. 6f, i; Fig. 7k) are also present. If in equilibrium and if barite is present, Ohmoto and Rye (1979) show that S isotopic compositions decrease as follows: $\delta^{34}S_{barite} > \delta^{34}S_{fluid} > \delta^{34}S_{sulfide}$. Under this condition, the $\delta^{34}S$ values of hydrothermal fluid should be higher than the minimum $\delta^{34}S$ value of sulfides i.e., $\delta^{34}S_{fluid} > 27.66‰$ or 24.80‰ (minimum S isotope values in Limei and Yutang, respectively). Such heavy S isotopic signatures are significantly higher than that reported for mantle-derived magmatic sulfur (~0‰; Ohmoto and Rye, 1979; Chaussidon et al., 1989), but overlap with those of the sulfate-bearing (e.g., barite) evaporates within Cambrian marine sedimentary in the region (Fig. 11); $\delta^{34}S$=+31.13 to + 37.30‰; Zhou et al., 2016; Wei et al., 2017) and the Ediacaran to Cambrian marine sulfate (+25 to + 35‰; Claypool et al., 1980). This finding is also supported by geological evidence. Sulfate-bearing dolostone (containing barite and/or gypsum) was identified in the middle to upper Cambrian sedimentary strata and their thickness is >1000 m (Li, 1991). Thus, the sulfate-bearing evaporates within Cambrian marine sedimentary are considered as a potential sulfur source for the Limei and Yutang deposits. Similar conclusion has been drawn for most nearby early Cambrian carbonate-hosted Pb-Zn deposits (Fig. 11), such as Shizishan (Duan, 2014) Danaopo (Wu et al., 2021), Shizishan (Duan, 2014) Niujiaotang (Ye et al., 2005, 2012), Tangbianpo (Yu et al., 2017), Bokouchang (Cai et al., 2014) and Xiunao (Cai et al., 2014; Li, 2018) in the XQMB, South China.

5.2.2. *Formation mechanism of reduced S*

Sulfate reduction is commonly caused by reaction with hydrocarbons, either through abiotic thermochemical processes or bacterially mediated processes (Seal, 2006). Both bacterial sulfate reduction (BSR) and thermochemical sulfate reduction (TSR) occur in two mutually exclusive thermal regimes. The upper limit for effective BSR is approximately 30 to 40 °C (Jørgensen et al., 1992) and it can produce

sulfate–sulfide fractionations between 15 and 60‰ (Goldhaber and Kaplan, 1975) with negative $\delta^{34}S$ values of reduced sulfur. At Limei and Yutang, however, the homogenization temperature of fluid inclusions in ore minerals (e.g., sphalerite and calcite) are higher than 100 °C (Liu and Zheng, 2000). Moreover, the range of $\delta^{34}S$ values of sulfides from S1–2 are strongly positive, from + 27.66 to + 35.46‰ at Limei and + 24.80 to + 36.07‰ at Yutamg, respectively. Therefore, BSR probably did not occur, at least during the formation of S^{2-} from SO during sulfide precipitation at Limei and Yutang. It is worth noting that the optimum temperature of TSR is generally > 120 °C and it produces sulfate–sulfide fractionations from 0 to 15‰ (Goldhaber and Kaplan, 1975; Ohmoto and Rye, 1979) that matches with the observed S isotopic ranges of Limei and Yutang. Meanwhile, bioclastic limestone and organic matter in ore-hosting strata (Fig. 6a–b, k; Fig. 7c,i) serve as reducing agents during TSR happen. Therefore H_2S could be produced from sulfates through the reactions of $SO + 2C = S^{2-} + 2CO_2$, $SO + CH_4 = H_2S + CO + H_2O$ or $SO + 2CH_2O = H_2S + 2HCO$ (Machel et al., 1995). Overall, we consider that TSR played a critical role in forming reduced sulfur in the Limei and Yutang deposits.

5.2.3. Microscale S isotope variation

Many studies have demonstrated that microscale variations in $\delta^{34}S$ values of sulfur-bearing minerals determined by in situ analysis can provide new insights into the ore-forming process that cannot be resolved by bulk S isotopic compositions alone (e.g., Peevler et al., 2003). This is because sulfur isotopic compositions obtained by traditional sampling techniques (micro-drilling or mineral separation) preclude the ability to analyze compositions based on textual variation (nm) in sphalerite.

Microscale variations in $\delta^{34}S$ values exist among different grains and even within single sphalerite grains, which can be explained by: (i) variations of physical–chemical conditions (such as *T*, pH and fO_2) of hydrothermal fluids; (ii) mixtures of multiple S reservoirs; and (iii) the $\delta^{34}S$ compositions of H_2S responsible for precipitating sulfides (Ohmoto and Rye, 1979; Seal, 2006). As mentioned earlier, the homogenization temperature of fluid inclusions in ore minerals (i.e., sphalerite and calcite) span a considerable range, i.e., 120–200 °C at Limei and 92–170 °C at Yutang (Liu and Zheng, 2000), suggesting appreciable temperature fluctuations during sulfide precipitation. Given that S isotopic fractionation between H_2S and ZnS/FeS_2 is insignificant and virtually independent of temperature (Kajiwara and Krouse, 1971), observed $\delta^{34}S$ variations are interpreted to be unrelated to temperature. Meanwhile, there are the relative metastable environment, particularly pH and fO_2 during Pb-Zn mineralization by the circulating process of carbonate dissolution → re-precipitation. Under this condition, the physical–chemical conditions (such as *T*, pH and fO_2) could not be a significant factor in producing the observed $\delta^{34}S$ variation in single sphalerite grain. As shown by early studies, the mixing of ^{34}S-enriched fluid and ^{34}S-depleted fluid can cause significant variations in S isotope compositions (Seal, 2006). In situ S isotopic data in this study show a narrow range (+27.66 to + 35.46‰ at Limei and + 24.80 to + 36.07‰ at Yutamg, respectively). Furthermore, the ^{34}S values in sulfides increase and then decrease in single sphalerite grains from core to rim (Fig. 7j). Additionally, many authors suggest that the reduced sulfur from the carbonate-hosted Pb-Zn deposits in the XQMB, South China was derived from a single S reservoir, i.e., sulfate-bearing evaporates within Cambrian sedimentary strata (Ye et al., 2005, 2012; Cai et al., 2014; Zhou et al., 2017; Yu et al., 2017; Li et al., 2017). Therefore, it is likely that the observed $\delta^{34}S$ variation of sulfides among different ore stages may be brought about by the S composition in the original fluid.

5.3. Source(s) of metals

Considering that the U and Th contents in sulfides (such as pyrite, sphalerite and galena) are negligible, Pb isotope ratios of these minerals formed from different paragenetic stages likely reflect the original Pb isotope composition of hydrothermal fluids (Schneider et al., 2002; Ayuso et al., 2004). In this study, in situ Pb isotopic ratios of sulfides from S1–2 of Limei and Yutang were determined and results show that their Pb isotope ratios are collinear (with analytical error) on both $^{207}Pb/^{204}Pb$ vs. $^{206}Pb/^{204}Pb$ and $^{208}Pb/^{204}Pb$ vs. $^{206}Pb/^{204}Pb$ diagrams (Fig. 12c–d). Such linear relationships may be explained by differential leaching and extraction of radiogenic Pb from a homogeneous regional source (Sverjensky et al., 1979; Field et al., 2018) or well mixing of two distinct source-rock components characterized by different Pb isotope values at the site of deposition (Schneider et al., 2002; Ayuso et al., 2004). The implications of these two interpretations are considered separately below.

If all lead was derived from a homogeneous regional source, the sulfides would inherit the relatively homogeneous Pb isotope compositions from metal sources (Sverjensky et al., 1979; Field et al., 2018). In the case of the Limei and Yutang deposits, some of the Pb isotope ratios of sulfides fall outside of the age-corrected field for the Proterozoic metamorphic basement (Banxi Gp.), which suggests that a homogeneous regional source (basement rocks) is unlikely to have caused the observed linear trend of Pb data of sulfides (Fig. 12a–b) because that the relatively radiogenic Pb isotope ratios cannot be produced from a source with lighter Pb isotope ratios. It is more likely that the observed Pb isotope ratios of sulfide minerals are due to the mixing of two or more end-member compositions. The fact that the majority of Pb isotope compositions of sulfide samples fall into the age-corrected field of Banxi Gp. rocks, suggesting that it is an important source of Pb for the Limei and Yutang deposits (Zhou et al., 2016; Wei et al., 2017 and this study), but early Cambrian sedimentary strata (host rocks and underlying Shipai and Niutitang Fms.) could be another possible source of lead because that they have relatively higher Pb isotope ratios (Fig. 12a–b).

In terms of changes in Pb isotope ratios during evolution of the fluids, the Pb isotopic ratios increase from early ore-stage (S2) to the late phase (S3), suggesting that increasingly radiogenic Pb sources perhaps the early Cambrian sedimentary rocks (Fig. 12c–d), provided more Pb for the ore-forming fluids during the later stages. Due to low Pb and Zn concentrations in these rocks (data from Appendix Table 3, Liu et al. 2012), early Cambrian sedimentary strata cannot contribute sufficient amount of Pb that causes large variation of Pb isotope ratios with the Limei and Yutang deposits. This finding is supported by the Sr isotopes of country rocks in the XQMB. The Sr isotope ratios of age-corrected (410 Ma) ore minerals (e.g., calcite and sphalerite) from Limei and Yutang are lower than the metamorphic basement, early Cambrian Shipai and Niutitang Fms., but are higher than those of the host rocks (Fig. 13) suggesting a mixture source of older basement and early Cambrian sedimentary strata. Hence, the Proterozoic metamorphic basement provides the main metal sources for the Limei and Yutang deposits with an amount of contribution from the early Cambrian sedimentary strata via fluid-rock reaction.

5.4. Mechanism(s) of sulfide ore deposition

Sulfide precipitation mechanisms are commonly explained in one of three models:(1) reduced sulfur; (2) local sulfate reduction; and (3) two-fluid mixing (Leach et al., 2005). The first model calls for metals and reduced sulfur to be transported together in an acidic fluid (pH < 4.5) at temperatures > 200 °C, and precipitation is caused by cooling, pH changes, fluid dilution and wall-rock alteration (Anderson, 1975). Model 2 involves transports of metals and oxidized sulfur (SO) in the same fluid; with sulfate being reduced by reductants (e.g., bitumen, methane, oil, etc.) at the depositional site (e.g., Beales, 1975). The last proposed mechanism calls for, mixing of a metal-bearing fluid and an enriched reduced sulfur fluid, with sulfate being reduced in a location remote from the ore depositional site (e.g., Beales, 1995; Corbella et al., 2004). Considering the low mineralization temperature of the Huayuan orefield (<200 °C), a carbonate-dominated (buffered near-natural pH) environment, low contents of CO_2 (e.g., Liu and Zheng, 2000; Li, 2018),

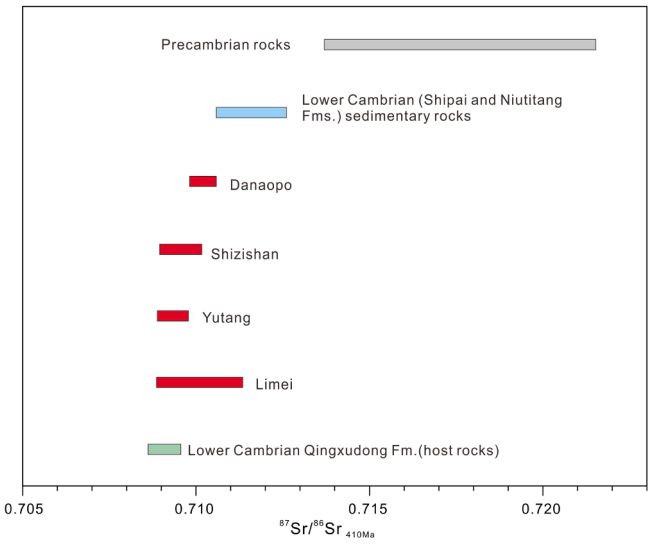

Fig. 13. Plot of $(^{87}Sr/^{86}Sr)_t$(t = 410 Ma) ratios for the early Cambrian carbonate-hosted Pb-Zn deposits, Precambrian rock, Lower Cambrian (Qingxudong, Shipai and Niutitang Fms.) sedimentary strata. Strontium isotopic data from Schneider et al. (2002), Peng et al. (2003), Duan (2014), Zhou et al. (2016) and Wei (2017).

and the lack of silicate minerals (such as quartz) coexisting with sulfide (Figs. 6–7), model 1 can be safely ruled out. As mentioned above, sulfur isotope data suggests that sulfate-bearing evaporates within Cambrian marine sedimentary were the main sulfur source for the Limei and Yutang deposits, whereas the metals were mainly derived from Proterozoic metamorphic basement rocks, which suggests that metals and reduced sulfur did not travel together in the single ore fluid. Therefore, model 3, the mixing of two fluids, is considered the most likely mechanism for sulfide deposition mechanism for the Limei and Yutang deposits. This model is also supported by geological evidence. The acid generated by fluid mixing causes carbonate dissolution, collapse features and carbonation shown in Fig. 6. In addition, the grade of sulfide ores shows a close spatial relationship with the intensity of sulfide-bearing evaporates (Duan, 2014).

5.5. Ore genesis

Sulfide orebodies at Huayuan occur as stratiform and/or lentiform and in conformable contact with the host rocks, leading to several authors to suggest it syngenetically formed (Luo et al., 2009; Chen et al., 2011) or sedimentary reworked type (Li, 1991; Mao, 2016). The near-vertical sulfide-bearing veins recently discovered in the district (Wei et al., 2020) and Rb-Sr dating of sphalerite suggests that Limei and Yutang were formed at 412 ± 6 Ma (MSWD = 1.5) and 410 ± 12 Ma (MSWD = 2.2), respectively, suggests an epigenetic origin for these deposits (Duan, 2014; Tan et al., 2018).

Many studies have suggested that the most important geological characteristics of carbonate-hosted Pb-Zn deposits in the XQMB (Liu and Zheng, 2000; Zhou et al., 2016; Li, 2018) are: (1) deposits are hosted in reef limestone; (2) there is no genetic relationship with igneous activity; (3) the deposits occur in platform carbonate sequences within a foreland basin; (4) low ore grades (<10 wt% Zn + Pb) dominated by Zn with minor Pb characterizes the deposits; (5) most deposits in the district cover hundreds of square kilometers; (6) mineral assemblages are simple with the dominant minerals being sphalerite, galena, calcite, hydrothermal dolomite with minor pyrite, fluorite and barite; and (7) associated alteration consists mainly of dolomitization, host-rock dissolution and brecciation. All these geological features are comparable with that of typical MVT deposits worldwide (Leach and Sangster, 1993; Leach et al., 2005). Based on the combined geologic and geochemical evidence, the Limei and Yutang deposits in the Huayuan orefield are likely epigenetic MVT deposits.

5.6. Metallogenic model for regional Pb-Zn mineralization

It is generally accepted that the MVT Pb-Zn mineralization formed in large contractional tectonic events during nearby orogenic activity (e.g., Leach and Rowan, 1986; Bradley and Leach, 2003). Radiogenic isotope geochronological data indicate that the Pb-Zn deposits in the XQMB hosted in early Cambrian carbonate rocks formed in the early Ordovician to early Devonian (410–490 Ma; Table 1; Duan, 2014; Yang et al., 2015; Yu et al., 2017; Tan et al., 2018), a period that was contemporaneous with the Wuyi–Yunkai orogenic event in the study area (e.g. Yao and Li, 2016; Wei et al., 2020). These ages together with the important geological and geochemical characteristics of these MVT deposits and the tectonic evolution of the study region have allowed us to construct a genetic model for the Pb-Zn mineralization in the XQMB.

The Wuyi–Yunkai orogeny caused the formation of the Nanhua foreland basin, located at the study area since at least Ordovician (Yao and Li, 2016) and developed a series of NE- and NNE-trending structures and the subsidiary NW-trending faults (e.g., Wang et al., 2013). As shown in Fig. 14, hydrothermal metalliferous fluids were expelled by the Wuyi-Yunkai compressional event and migrated from the marginal sediments into the foreland basin. Metal-bearing fluids ascended through basement rocks and into the porous Cambrian reef limestone, along steeply dipping NE- NNE-trending faults, i.e., Huayuan–Zhangjiajie fault. When the fluids encountered the reduced sulfur from the evaporitic sulfates within Cambrian sediment strata, the mixing of metal-bearing fluids formed acidic solutions (e.g., $MeCl_{(aq)} + H_2S_{(aq)} = MeS_{(s)} + H^+ + 4Cl^-$; where Me is Zn, Pb, etc.) along bedding-plane faults. The interaction of acidic solution with surrounding carbonate rocks creates new spaces for sulfide precipitation and forms the stratiform replacement orebodies.

6. Conclusions

In the Limei and Yutang deposits, Huayuan orefield, the following conclusions could be reached based on geological, mineralogical evidence and the new fluorite REY geochemistry and sulfides in situ S-Pb isotopes data presented here:

(1) REY geochemistry indicates that REEs and metals were transported predominantly as chloride complexes in a low-temperature hydrothermal fluid (<200 °C) for Limei and Yutang.
(2) Reduced sulfur was mainly derived from TSR of the evaporite sulfate within the early Cambrian sedimentary strata. Sulfides in the hydrothermal stage show various $\delta^{34}S$ values (up to 11.27‰) even in single grains (up to 4.60‰), which are mainly attributed to the $\delta^{34}S$ values of original fluid.
(3) The source of Pb (and by inference other metals) was mainly derived from the Proterozoic metamorphic basement. The early Cambrian sedimentary rocks (e.g., bioclastic limestone, organic matter) not only act as the reducing agent for TSR but also provide further facilitate the sulfide precipitation.
(4) The Wuyi–Yunkai orogeny drove large scale fluid migration, resulting in sulfide precipitation in the Limei and Yutang deposits, reflecting the mixing of two fluids: one is poor in reduced sulfur but rich in metals (flowed through the Proterozoic metamorphic basement and underlying sedimentary strata) and the other is rich in reduced sulfur but poor in metal (derived from host rocks).

Declaration of Competing Interest

The authors declare that they have no known competing financial interests or personal relationships that could have appeared to influence

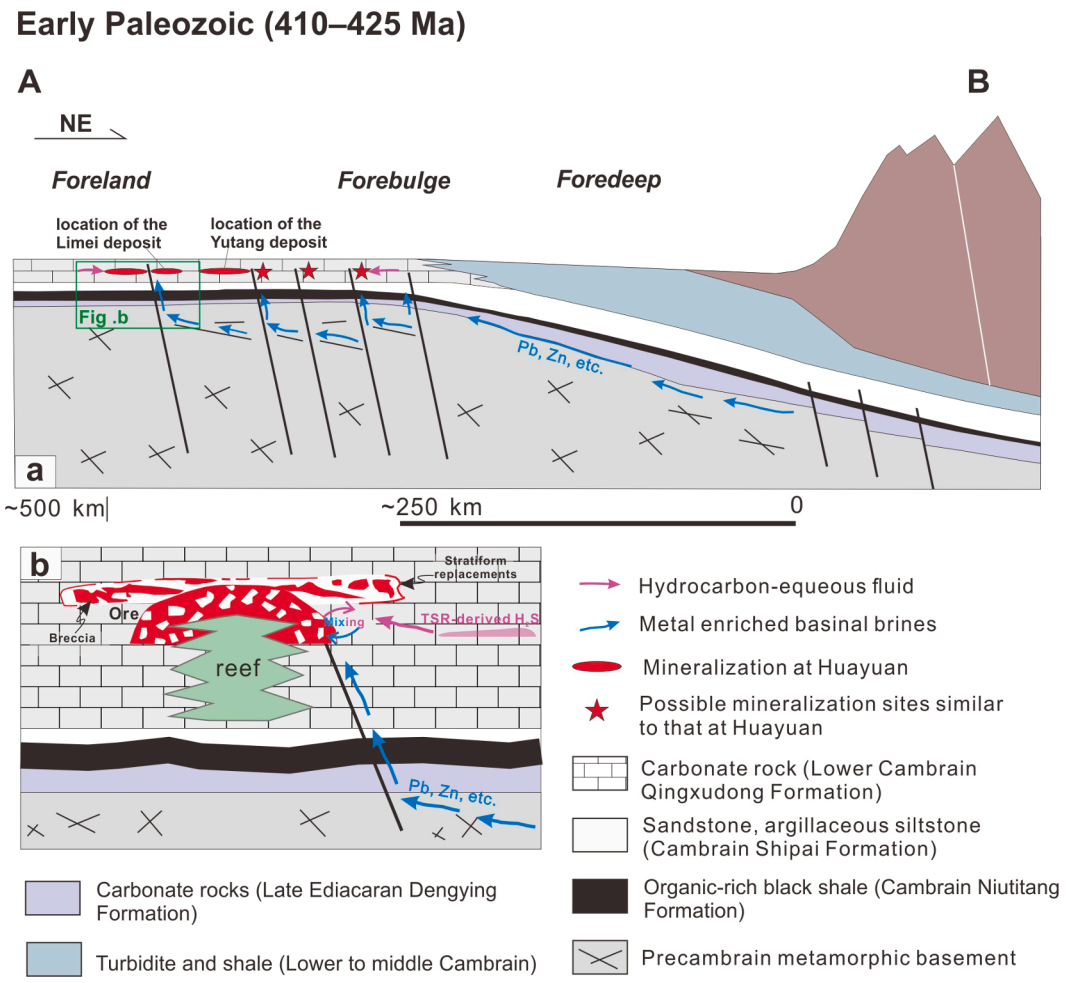

Fig. 14. Genetic model for the Limei and Yutang deposits in a foreland basin setting during the Wuyi–Yunkai orogenic activity. (a) Paleotectonic setting during the Pb-Zn mineralization at Huayuan. NW-SE palecross-section A–B (Fig. 1) showing the location of the present-day Limei and Yutang deposits. (b) Close-up of the mineralization process at Limei.

the work reported in this paper.

Acknowledgements

This work was financially supported by the National Natural Science Foundation of China (42173025, 92162218, and U1812402) and the Natural Science Foundation of Guizhou Province ([2021]123). The authors thank Mr. Jiankang Zeng for assistance in field sampling. Dr. Jing Hu at IGCAS and Zhi-An Bao and Kai-Yun Chen at Northwestern University, Xi'an were indebted for helping with trace elements and in situ S-Pb isotopes analysis, respectively. We also thank two anonymous reviewers for detailed and constructive reviews and editors Franco Pirajno and Hao Zou for editorial handling, which all helped improve the paper.

Appendix A. Supplementary data

Supplementary data to this article can be found online at https://doi.org/10.1016/j.oregeorev.2021.104682.

References

Anderson, G.M., 1975. Precipitation of Mississippi Valley-type ores. Econ. Geol. 70, 937–942.
Ayuso, R.A., Kelley, K.D., Leach, D.L., Young, L.E., Wandless, J.F.S., Lyon, A.M., Dillingham, J.L., 2004. Origin of the Red Dog Pb-Zn-Ag deposits, Brooks Range, Alaska: Evidence from regional Pb and Sr isotope sources. Econ. Geol. 99 (7), 1533–1553.
Bao, Z., Yuan, W., Yuan, H., Liu, X.u., Chen, K., Zong, C., 2016. Non-matrix-matched determination of lead isotope ratios in ancient bronze artifacts by femtosecond laser ablation multi-collector inductively coupled plasma mass spectrometry. Int. J. Mass Spectrom. 402, 12–19.
Bau, M., Dulski, P., 1995. Comparative study of yttrium and rare-earth element behaviors in fluorine-rich hydrothermal fluids. Contrib. Mineral. Petrol. 119 (2–3), 213–223.
Bau, M., Romer, R.L., Lüders, V., Dulski, P., 2003. Tracing element sources of hydrothermal mineral deposits: REE and Y distribution and Sr-Nd-Pb isotopes in fluorite from MVT deposits in the Pennine orefield, England. Miner. Deposita 38 (8), 992–1008.
Beales, F.W., 1975. Precipitation mechanisms for Mississippi Valley-type ore deposits. Econ. Geol. 70, 943–948.
Bouabdellah, M., Fontbote, L., Haeberlin, Y., Llinares, L., Leach, D., Pangenberg, J., 1999. Zoned sulfur isotope signatures at the Mississippi Valley-type Toussit Bou Beker, El Abed district, Morocco, Algeria—evidence for thermochemical sulfate reduction and mixing of sulfur sources. In: Stanley, C.J. (Ed.), Mineral deposits: Processes to processing: Rotterdam, Balkema, pp. 821–824.
Bradley, D.C., Leach, D.L., 2003. Tectonic controls of Mississippi Valley-type lead-zinc mineralization in orogenic forelands. Miner. Deposita 38, 652–667.
Cai, Y.X., Yang, H.M., Duan, R.C., Lu, S.S., Zhang, L.G., Liu, Z.F., Qiu, X.F., 2014. Fluid inclusions and S, Pb, C isotope geochemistry of Pb-Zn deposits hosted by Lower Cambrian in Western Hunan-Eastern Guizhou area. Geoscience 28 (1), 30–41 (in Chinese with English abstract).
Charvet, J., 2013. The Neoproterozoic-early Paleozoic tectonic evolution of the South China Block: an overview. J. Asian Earth Sci. 74, 198–209.
Chaussidon, M., Albarède, F., Sheppard, S.M.F., 1989. Sulphur isotope variations in the mantle from ion microprobe analyses of micro-sulphide inclusions. Earth Planet. Sc. Lett. 92 (2), 144–156.
Chen, L.u., Chen, K., Bao, Z., Liang, P., Sun, T., Yuan, H., 2017. Preparation of standards for in situ sulfur isotope measurement in sulfides using femtosecond laser ablation MC-ICP-MS. J. Anal. Atom Spectrom. 32 (1), 107–116.
Chen, M.H., Hu, X.Z., Bao, Z.X., Bao, J.M., 2011. Geological features and metallogenesis of the Yutang Pb-Zn ore concentration belt in Hunan Province. Geol. Explor. 47 (2), 251–260 (in Chinese with English abstract).

Chen, Y.P., Xiang, N., Tang, Q., Ma, C.C., 2018. Geological characteristics and metallogenic geological conditions of Danaopo Zn-Pb deposit in western Hunan. Miner. Explor. 9, 1127–1133 (in Chinese with English abstract).
Claypool, G.E., Holser, W.T., Kaplan, I.R., Sakai, H., Zak, I., 1980. The age curves of sulfur and oxygen isotopes in marine sulfate and their mutual interpretation. Chem. Geol. 28, 199–260.
Corbella, M., Ayora, C., Cardellach, E., 2004. Hydrothermal mixing, carbonate dissolution and sulfide precipitation in Mississippi Valley-type deposits. Miner. Deposita 39 (3), 344–357.
Duan, Q.F., 2014. The research of metallogenic regularity of stratabound zinc-lead deposits from Sinian-Cambrian in Weatern Hunan and Western Hubei. Ph.D. Dissertation. China University of Geosciences, Wuhan (in Chinese with English abstract).
Fang, Y.i., Zou, H., Bagas, L., Said, N., Li, Y., Liu, H., 2020. Fluorite deposits in the Zhejiang Province, southeast China: the possible role of extension during the late stages in the subduction of the Paleo-Pacific oceanic plate, as indicated by the Gudongkeng fluorite deposit. Ore. Geol. Rev. 117, 103276.
Field, J.D., Appold, M.S., Renson, V., Coveney, R.M., 2018. Lead and sulfur isotope composition of trace occurrences of Mississippi Valley-type mineralization in the U. S. midcontinent. J. Geochem. Explor. 184, 66–81.
Fu, S., 2011. Discussion on formation rules of high-grade Pb-Zn ore in western Hunan Nonferrous Metal Mining. Sec. 63 (6), 27–35 (in Chinese with English abstract).
Goldhaber, M.B., Kaplan, I.R., 1975. Controls and consequences of sulfate reduction rates in recent marine sediments. Soil Sci. 119 (1), 42–55.
Han, R.S., Hu, Y.Z., Wang, X.K., Hou, B.H., Huang, Z.L., Chen, J., Wang, F., Wu, P., Li, B., Wang, H.J., Dong, Y., Lei, L., 2012. Mineralization model of rich Ge–Ag-bearing Zn–Pb polymetallic deposit concentrated district in northeastern Yunnan, China. Acta. Geol. Sin-Engl. 86, 280–294 (in Chinese with English abstract).
Heijlen, W., Muchez, P., Banks, D.A., Schneider, J., Kucha, H., Keppens, E., 2003. Carbonate-hosted Zn-Pb deposits in Upper Silesia, Poland: origin and evolution of mineralizing fluids and constraints on genetic models. Econ. Geol. 98 (5), 911–932.
Hu, R.Z., Mao, J.W., Hua, R.M., Fan, W.M., 2015. Intra-continental mineralization of South China Craton. Science Press, Beijing 1–903 (in Chinese).
Hu, Y.S., Ye, L., Wei, C., Huang, Z.L., Wang, H.Y., 2020. REE geochemistry of the hydrothermal calcites from the Huayuan orefield, in the western Hunan, China. Acta Mineral. Sin. 40 (4), 441–449 (in Chinese with English Abstract).
Huang, Z.L., Chen, J., Han, R.S., Li, W.B., Liu, C.Q., Zhang, Z.L., Ma, D.Y., Gao, D.R., Yang, H.L., 2004. Geochemistry and ore-formation of the Huize giant lead-zinc deposit, Yunnan Province, China: Discussion on the relationship between Emeishan flood basalts and lead-zinc mineralization. Geol. Pub. House, Beijing, 1–154 (in Chinese).
Jørgensen, B.B., Isaksen, M.F., Jannasch, H.W., 1992. Bacterial sulfate reduction above 100°C in deep-sea hydrothermal vent sediments. Science 258 (5089), 1756–1757.
Kajiwara, Y., Krouse, H.R., 1971. Sulfur isotope partitioning in metallic sulfide systems. Can. J. Earth Sci. 8 (11), 1397–1408.
Leach, D.L., Sangster, D.F., 1993. Mississippi Valley-type lead-zinc deposits. In: Kirkham, R.V., Sinclair, W.D., Thorpe, R.I., and Duke, J.M., (eds.). Mineral Deposit Modeling. Geological Association of Canada Special Paper, 40, 289–314.
Leach, D.L., Rowan, E.L., 1986. Genetic link between Ouachita foldbelt tectonism and the Mississippi Valley-type lead-zinc deposits of the Ozarks. Geology 14 (11), 931–935.
Leach, D.L., Sangster, D.F., Kelley, K.D., Large, R.R., Garven, G., Allen, C.R., Gutzmer, J., Walters, S., 2005. Sediment-hosted lead-zinc deposits: a global perspective. Econ. Geol. 100th Anniv, 561–607.
Leach, D.L., Song, Y.C., 2019. Sediment-Hosted Zinc-Lead and Copper Deposits in China. SEG Spec. Pub. 22, 325–409.
Li, Z.F., 1991. A preliminary discussion on the origin of Pb-Zn ore deposits in western Hunan and eastern Guizhou. Guizhou Geol. 8 (4), 363–371 (in Chinese with English abstract).
Li, K., Duan, Q.F., Zhao, S.R., Tang, Z.Y., 2017. Material sources and ore-forming mechanism of the Huayuan Pb-Zn ore deposit in Hu'nan Province: evidence from S, Pb, Sr isotopes of sulfides. Geol. Bull. China 36 (5), 811–822 (in Chinese with English abstract).
Li, Z.X., Li, X.H., Wartho, J.A., Clark, C., Li, W.X., Zhang, C.L., Bao, C.M., 2010. Magmatic and metamorphic events during the Early Paleozoic Wuyi-Yunkai orogeny, southeastern South China: new age constraints and P-T conditions. GSA Bull. 122 (5–6), 772–793.
Li, K., 2018. Metallogenic Model and Prediction of the Carbonate-Hosted Pb-Zn deposits in Western Hunan and Eastern Guizhou Province, South China. Ph.D. dissertion. China University of Geosciences, Wuhan (in Chinese with English abstract).
Liu, W.J., Zheng, R.C., Li, Y.L., Chang, S.H., 1997. Research of the daughter minerals in fluid inclusions of the Huayuan lead-zinc deposit. J. Chengdou Univ. Tech. 24 (4), 65–69 (in Chinese with English abstract).
Liu, W.J., Zheng, R.C., 2000. Characteristic and movement of ore-forming fluids in the Huayuan lead-zinc deposit. Mineral. Depos. 19 (2), 173–181.
Liu, J.S., Zou, X.W., Tang, C.Y., Cui, S., Xia, J., Gan, J.M., Zhou, W.Q., Jin, S.C., 2012. Preliminary discussion on relationship between Pb-Zn deposits and paleo-oil reservoirs in western Hunan and eastern Guizhou Province. Geol. Mineral. Resour. South China 28 (3), 220–225 (in Chinese with English abstract).
Luo, W., Yin, Z., Kong, L., Dai, T.G., 2009. Discussion on the geological features and genesis of the Limei Pb-Zn ore concentration belt in northwestern Hunan Province. Geol. Survey Res. 32 (3), 194–202 (in Chinese with English abstract).
Machel, H.G., Krouse, H.R., Sassen, R., 1995. Products and distinguishing criteria of bacterial and thermochemical sulfate reduction. Appl. Geochem. 10 (4), 373–389.
Mao, D.L., 2016. Geological characteristics and genesis of the Danaopo Pb-Zn deposit in Huayuan County, Hunan Province. Modern Mining 32 (2), 90–94, 97 (in Chinese with English abstract).
Metcalfe, I., 2006. Palaeozoic and Mesozoic tectonic evolution and palaeogeography of East Asian crustal fragments: The Korean Peninsula in context. Gondwana Res. 9 (1-2), 24–46.
Migdisov, A.A., Williams-Jones, A.E., 2007. An experimental study of the solubility and speciation of neodymium (III) fluoride in F-bearing aqueous solutions. Geochim. Cosmochim. Acta 71 (12), 3056–3069.
Migdisov, A.A., Williams-Jones, A.E., Wagner, T., 2009. An experimental study of the solubility and speciation of the rare earth elements (III) in fluoride- and chloride-bearing aqueous solutions at temperatures up to 300°C. Geochim. Cosmochim. Acta 73 (23), 7087–7109.
Ohmoto, H., Rye, R.O., 1979. Isotopes of sulfur and carbon. In: Barnes, H.L. (Ed.), Geochemistry of hydrothermal ore deposits. Wiley, New York, pp. 509–567.
Peevler, J., Fayek, M., Misra, K.C., Riciputi, L.R., 2003. Sulfur isotope microanalysis of sphalerite by SIMS: constraints on the genesis of Mississippi Valley-type mineralization, from the Mascot-Jefferson City district, East Tennessee. J. Geochem. Explor. 80 (2-3), 277–296.
Peng, J.T., Hu, R.Z., Zhao, J.H., Fu, Y.Z., 2003. The ore-forming fluid with a marked radiogenic ^{87}Sr signature from the Woxi Au-Sb-W Deposit and its significant implications. Bull. Mineral. Petrol. Geochem 22 (3), 193–196 (in Chinese with English abstract).
Powell, T.G., MacQueen, R.W., 1984. Precipitation of sulfide ores and organic matter: sulfate reactions at Pine Point. Canada Sci. 224 (4644), 63–66.
Qi, L., Hu, J., Gregoire, D.C., 2000. Determination of trace elements in granites by inductively coupled plasma mass spectrometry. Talanta 51, 507–513.
Randell, R.N., Anderson, G.M., 1996. Geology of the Polaris Zn-Pb deposit and surrounding area, Canadian Arctic Archipelago. Soc. Econ. Geol. Spec. Pub. 4, 307–319.
Schneider, J., Boni, M., Lapponi, F., Bechstadt, T., 2002. Carbonate-hosted zinc-lead deposits in the lower Cambrian of Hunan, south china: a radiogenic (Pb, Sr) isotope study. Econ. Geol. 97 (8), 1815–1827.
Seal, R.R., 2006. Sulfur isotope geochemistry of sulfide minerals. Rev. Mineral. Geochem. 61 (1), 633–677.
Souissi, F., Sassi, R., Dandurand, J.L., Bouhlel, S., Ben Hamda, S., 2007. Fluid inclusion microthermometry and rare earth element distribution in the celestites of the Jbel Doghra ore deposit (Dome zone, northern Tunisia): Towards a new genetic model. Bull. Société Géol. France 178 (6), 459–471.
Sun, S.S., McDonough, W.F., 1989. Chemical and isotopic systematic of oceanic basalts: implications for mantle compositions and processes, in Saunders, A.D., Norry, M.J., eds. Magmatism in the ocean basins. Geol. Soc. Spec. Pub. 42, 313–345.
Sverjensky, D.A., Rye, D.M., Doe, B.R., 1979. The lead and sulfur isotopic compositions of galena from a Mississippi Valley-Type Deposit in the New lead Belt, southeast Missouri. Econ. Geol. 74 (1), 149–153.
Tan, J.J., Liu, C.P., Yang, H.M., Cai, Y.X., Lu, S.S., 2018. Geochronology and ore-forming material source constraints for Rouxianshan Pb-Zn deposit in Huayuan ore concentration area, western Hunan. Earth Sci. 43 (7), 2438–2448 (in Chinese with English abstract).
Tang, C.Y., Deng, F., Li, K., Wang, G.Q., Duan, Q.F., Zou, X.W., Zhao, W.Q., Jin, S.C., 2012. Sedimentary sequence of the Lower Cambrian Qingxudong Formation in the western Hunan and eastern Guizhou Provinces and its constrains on lead-zinc mineralization. Geotect. Metall. 36 (1), 111–117 (in Chinese with English abstract).
Wang, Y., Fan, W., Zhang, G., Zhang, Y., 2013. Phanerozoic tectonics of the South China Block: Key observations and controversies. Gondwana Res 23 (4), 1273–1305.
Wang, J., Li, Z.X., 2003. History of Neoproterozoic rift basins in South China: implications for Rodinia break-up. Precambrian Res. 122, 141–158.
Wei, C., Huang, Z., Ye, L., Hu, Y., Santosh, M., Wu, T., He, L., Zhang, J., He, Z., Xiang, Z., Chen, D.a., Zhu, C., Jin, Z., 2021. Genesis of carbonate-hosted Zn-Pb deposits in the Late Indosinian thrust and fold systems: An example of the newly discovered giant Zhugongtang deposit, South China. J. Asian Earth Sci. 220, 104914. https://doi.org/10.1016/j.jseaes.2021.104914.
Wei, H.T., Shao, Y.J., Xiong, Y.Q., 2017. Metallogenic model of Huayuan Pb-Zn ore field in the western Hunan Province, South China. J. Cent. South Univ. 48 (9), 2402–2413 (in Chinese with English abstract).
Wei, H., Xiao, K., Shao, Y., Kong, H., Zhang, S., Wang, K., Li, Q., Chen, B., Xiang, J., Wen, C., 2020. Modeling-based mineral system approach to prospectivity mapping of stratabound hydrothermal deposits: a case study of MVT Pb-Zn deposits in the Huayuan area, northwestern Hunan Province, China. Ore Geol. Rev. 120, 103368. https://doi.org/10.1016/j.oregeorev.2020.103368.
Wei, H.T., 2017. Mineralization of the Huayuan Pb-Zn orefield, western Hunan. Ph.D. dissertion. Central South University, Changsha (in Chinese with English abstract).
Wu, T., Huang, Z., Ye, L., Wei, C., Chen, J., Yang, M.u., Yan, Z., Sui, Z., 2021. Origin of the carbonate-hosted Danaopo Zn-Pb deposit in western Hunan Province, China: Geology and in situ mineral S-Pb isotope constraints. Ore Geol. Rev. 129, 103941. https://doi.org/10.1016/j.oregeorev.2020.103941.
Yang, H.M., Liu, C.P., Duan, R.C., 2015. Rb-Sr and Sm-Nd isochron ages of Bokouchang Pb-Zn deposit in Tongren, Guizhou Province and their geological implication. Geotect. Metall. 39 (5), 855–865 (in Chinese with English abstract).
Yao, W.-H., Li, Z.-X., 2016. Tectonostratigraphic history of the Ediacaran-Silurian Nanhua foreland basin in South China. Tectonophysics 674, 31–51.
Ye, L., Pan, Z.P., Li, C.Y., Liu, T.G., Xia, B., 2005. Isotopic geochemical characters in Niujiaotang Cd rich zinc deposit, Duyun. Guizhou. J. Mineral. Petrol. 25 (2), 70–74 (in Chinese with English abstract).
Ye, L., Cook, N.J., Ciobanu, C.L., Yuping, L., Qian, Z., Tiegeng, L., Wei, G., Yulong, Y., Danyushevskiy, L., 2011. Trace and minor elements in sphalerite from base metal deposits in South China: A LA-ICPMS study. Ore Geol. Rev. 39 (4), 188–217.

Ye, L., Cook, N.J., Liu, T., Ciobanu, C.L., Gao, W., Yang, Y., 2012. The Niujiaotang Cd-rich zinc deposit, Duyun, Guizhou province, Southwest China: ore genesis and mechanisms of cadmium concentration. Miner. Deposita 47 (6), 683–700.

Yu, Y.S., Liu, A.S., Dai, P.Y., Zhao, W.Q., Tao, M., Liu, Z.F., 2017. The metallogenic epoch and ore-forming material source of the Tangbian Pb-Zn deposit in Tongren, Guizhou Province: Evidence from Rb-Sr dating of sphalerites and S-Pb isotope. Geol. Bull. China 36 (5), 885–892 (in Chinese with English abstract).

Zhang, C., Wu, Y., Hou, L., Mao, J., 2015. Geodynamic setting of mineralization of Mississippi Valley-type deposits in world-class Sichuan-Yunnan-Guizhou Zn-Pb triangle, southwest China: implications from age-dating studies in the past decade and the Sm-Nd age of Jinshachang deposit. J. Asian Earth Sci. 103, 103–114.

Zhao, J., Zhou, M.F., Yan, D., Zheng, J., Li, J., 2011. Reappraisal of the ages of Neoproterozoic strata in South China: No connection with the Grenvillian orogeny. Geology 39 (4), 299–302.

Zhou, Y., Duan, Q.F., Chen, Y.C., Tang, J.X., Cao, L., Peng, S.G., Gan, J.M., 2016. C, O, H, S, Pb and Sr isotope constraints on the sources of metals of Huayuan Pb-Zn deposits in western Hunan. Acta Geol. Sin. 90 (10), 2786–2802 (in Chinese with English abstract).

Zhou, Y., Duan, Q.F., Cao, L., Yu, Y.S., Peng, S.G., Gan, J.M., Li, K., Huang, H.L., Li, F., 2018b. Microthermometry and characteristic elements determination of the fluid inclusions of the Huayuan lead-zinc deposit in western Hunan. Earth Sci. 43 (7), 2465–2483 (in Chinese with English abstract).

Zhou, J.-X., Xiang, Z.-Z., Zhou, M.-F., Feng, Y.-X., Luo, K., Huang, Z.-L., Wu, T., 2018a. The giant Upper Yangtze Pb–Zn province in SW China: Reviews, new advances and a new genetic model. J. Asian Earth Sci. 154, 280–315.

Zou, H., Fang, Y.i., Zhang, S.-T., Zhang, Q., 2017. The source of Fengjia and Langxi barite–fluorite deposits in southeastern Sichuan, China: evidence from rare earth elements and S, Sr, and Sm–Nd isotopic data. Geol. J. 52 (3), 470–488.

Zou, H., Li, M., Bagas, L., Li, Y., Fang, Y.i., Cao, H.-W., Jiang, X.-W., Chen, H.-F., 2020. Fluid composition and evolution of the Langxi Ba-F deposit, Yangtze Block, China: New insight from LA-ICP-MS study of individual fluid inclusion. Ore Geol. Rev. 125, 103702. https://doi.org/10.1016/j.oregeorev.2020.103702.

Zou, H., Li, M., Santosh, M., Zheng, D.a., Cao, H.-W., Jiang, X.-W., Chen, H.-F., Li, Z.-Q., 2022. Fault-controlled carbonate-hosted barite-fluorite mineral systems: The Shuanghe deposit, Yangtze Block, South China. Gondwana Res. 101, 26–43.